NATIONAL TECHNICAL UNIVERSITY OF ATHENS

Faculty of Civil Engineering
Institute of Steel Structures

Seismic assessment of an R.C moment resistant frame designed via the Yield Frequency Spectra

Structural Analysis and Design of Earthquake Resistant Structures
(ADERS)

Lyritsakis Charilaos

A thesis presented for the degree of
Master of Science

Supervisor: Dimitrios Vamvatsikos
Athens, Greece
September 2017
EMK ME 2017/07

Lyritsakis Charilaos(2017)

Seismic assesment of an R.C moment resistant frame designed via the Yield Frequency
Spectra

Postgraduate Thesis

EMK ME 2017/07

Institute of Steel Structures, National Technical University of Athens, Greece

To my parents

NATIONAL TECHNICAL UNIVERSITY OF ATHENS
FACULTY OF CIVIL ENGINEERING
INSTITUTE OF STEEL STRUCTURES

POSTGRADUATE THESIS
EMK ME 2017/07

Seismic assesment of an R.C moment resistant frame designed via the Yield Frequency Spectra

Lyritsakis Charilaos
Supervisor:Vamvatsikos D.

Abstract

The moment resisting frames of a certain four story building are designed using the Yield Frequency Method in order to meet certain performance objectives. The present dissertation is concerned with the evaluation and assessment of the design. Moreover, of significant importance was the way the structure idealization was carried out and how different integration methods or simulation techniques can affect the response and the execution time. To this end, the open-source Finite Element Analysis software OpenSees[1] was used, along with MatLab procedures developed by D.Vamvatsikos for performing Incremental Dynamic Analysis.

---

[1] `http://opensees.berkeley.edu/`

Acknowledgements

With the completion of this thesis I fulfill my last obligation towards the conferment of the Master of Science Degree in Structural Engineering. I would like to thank my supervisor prof.Dimitris Vamvatsikos for his support throughout my occupation with this text, as well as beyond that. This work is somewhat half-finished due to unexpected events (both joyful and sad) and its completion in this form is achieved under conditions that extend way beyond my control, and with alot of pressure, almost two months after its presentation.

Nevertheless, looking at the big picture, I consider it an interesting trip that came to an end, and an honor to graduate from such a wonderful school and working with individuals that inspired me to pursue a doctoral degree.

Contents

List of Figures

List of Tables

Chapter 1

Introduction

1.1 Overview

Contemporary structural design and analysis methods are carried out within the framework of certain design rules, which can either act as a complementary source of help for the practicing engineer or constitute a subset of a legal framework for construction, as is the case with the Eurocodes. The philosophy of these design rules are to minimize or even bypass the need for more complex and rigorous examination of the structure, as would be the case of assuming some form of non-linear response for a given event. Moreover, little support is provided to the professional engineer when the objective is not the design of a new structure, but the assessment of an existing one. Because of this, an observable trend in the civil-structural engineering community over the last years is a focus towards a performance oriented design, along with the need for more sofisticated methods and technology for the assessment.

To this end, potential damage forms or *measures* have to be defined, followed a quantification of various levels of structural damage states -*Performance Objectives* (PO)- that correspond to them. These Damage Measures (DM) are expressions of structural response during a limit state event such as a strong earthquake or a cyclone and can be identified as *interstory drift angle*, *peak roof drift* or any other DM that the engineer considers critical for the performance. Given a set of limit state events, some form(s) of non-linear analysis is performed and mappings between DMs and the so-called Intensity Measures (IM) -such as the Peak Ground Acceleration (PGA) - are established. With sufficient response data at hand, and with the aid of statistical and probabilistic analysis, a more thorough evaluation of structural performance can be achieved by estimating if and how often the various POs are violated or being *exceeded* within a predefined time frame.

However, these data sets available to the engineer are results of complex analyses, which, not rarely, include the simulation of both material and geometrical non-linear behaviour, and as such, they are the product of different kinds of cumulative errors. Furthermore, the structure discretization, in the context of a *Finite Element Analysis* (FEA) and the type of elements chosen by the analyst can cause the computational cost of the analysis to skyrocket, with large models and in conjuction with demanding analyses (e.g non-linear dynamic) often stopping within the elastic range of the response due to convergence issues. Consequently, it can be clearly seen that the demand for enhanced accuracy as far as structural response is concerned leads to a layered process, where the analyst has to address the structure both as a physical object exposed in the hazard of its immediate environment and as an assembly of mathematical elements.

1.2   Objective

The purpose of the present text is the performance assessment of a 4-tory R.C moment resistant frame building designed using the Yield Frequency Spectra method[1] and the ASCE-7 and ACI 318 for the hazard representation and structural design respectively. To this end, two models are developed using OpenSees: one lumped plasticity model, where damage is confined at the end nodes of each element, and one distributed plasticity model, where damage is allowed to spread along the length of the element. With the intent to proceed with the significantly less complex model of lumped plasticity, focus at this first stage was to compare the response of these two models under non-linear static analyses and refine the former according to the feedback from the fiber model, mainly as far as the section cracking and generally pre-yielding evolution of the stiffness is concerned.

After a satisfactory match between the two models is established, we proceed with the Incemental Dynamic Analysis[2] of the lumped model and the assessment of the initial design, given specific performance objectives.

1.3   Chapter Layout

In the first chapter, a brief overview concerning the building and its design method is given.

The second chapter is concerned with the two different simulation approaches, namely, the lumped and the distributed plasticity models and highlights some important aspects of their implementation in OpenSees.

Chapter three is where the results of the non-linear incremental static analyses are illoustrated and discussed, followed by the refinement of the lumped plasticity model.

Assessment of the structure takes place in the final chapter, where results from IDAs are presented, along with a discussion about the performance objectives, using the San Jose hazard curve.

---

[1]*Performance-based seismic design via Yield Frequency Spectra*, D.Vamvatsikos & M.A.Aschheim (2014)

[2]*Incremental Dynamic Analysis*,D.Vamvatsikos & C.A.Cornell,(2001)

Chapter 2

Preliminary Design

2.1 The Building

2.1.1 Static System

The building under consideration[1] is designed to withstand lateral loads by activating two (for each direction) peripheral moment resisting frames, while the inner beams are simply supported on the adjacent columns (shear connection). The inner columns behave as gravity columns, carrying only axial loads. The edge beams of the pair of MRFs along the horizontal direction however are also simply supported, in order to prevent the columns at each of the four corners to develop biaxial moment.

2.1.2 Building Geometry
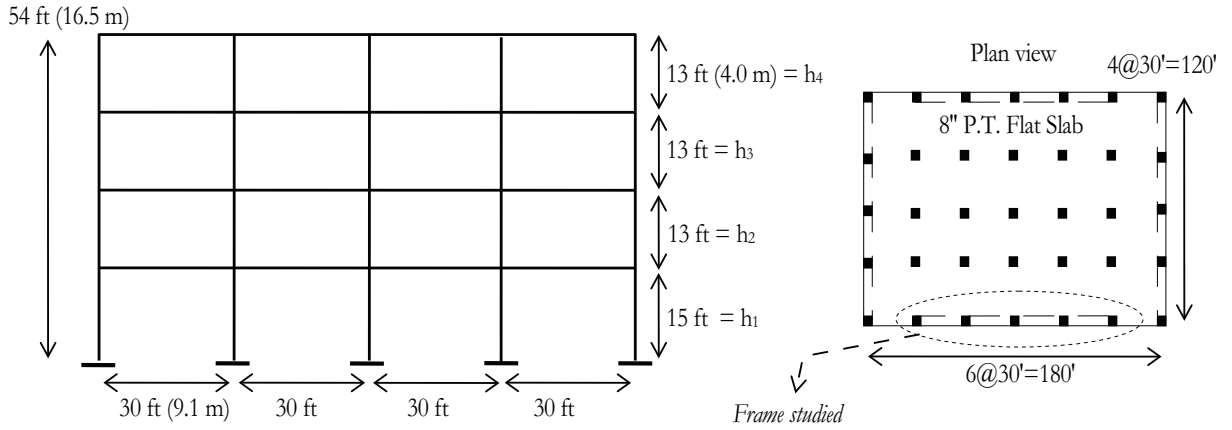
Figure 2.1: MRF elevation and building plan(Haselton)

As can be seen from Figure 2.1, the dimensions of the frame of interest are 120x54 (ftxft).It has four bays with each having a span of 30 ft. the first story height 15 ft and each floor beyond that at 13 ft. The slab width is 8 inches, same for each story.

2.1.3 Material properties and loading

The MRFs were designed using concrete of nominal strength $f_c = 5\,ksi$ and expected strength and modulus $f_{ce} = 6.5\,ksi$, $E_{ce} = 4595\,ksi$ respectively. For the steel of the rebars, the nominal yield strength is $f_y = 60\,ksi$, while the expected strength and yield strain are $f_{ye} = 69\,ksi$, $e_{ye} = 0.00238$. For the assessment, expected values were used.

The dead load per floor slab amounts to $q_{sl}^D = 175\,psf$ while live loads are assumed to be $q_{sl}^L = 50\,psf$. During seismic response, a quarter of the live loads is assumed present, thus resulting in a total slab load per floor $q_{sl} = q_{sl}^D + 0.25 \cdot q_{sl}^L \Rightarrow q_{sl} = 162.5\,psf$.

---

[1]Haselton(2006)

Therefore, the total (tributary) load per story during a seismic event, taking into account symmetry, is:

$$W_f = \frac{1}{2} \cdot (180 \; ft) \cdot (120 \; ft) \cdot q_{sl} \Rightarrow$$

$$W_f = 2025 \; kips$$

For the roof, only dead loads make up for the total gravity loads during seismic response:

$$W_f^{roof} = 1890 \; kips$$

2.1.4 Performance Objectives

The performance objectives are the following:

- System ductility limit at the 2/50 level is 3.6

- Interstory drift limit of 0.02

2.2 Initial Design using YFS and evaluation

The initial design of the MRF was carried out and provided by prof. Mark Aschheim using the **Yield Frequency Spectra** method. Using certain assumptions regarding the yield drift and the capacity curve of the equivalent SDOF system of the structure, the YFS method associates the mean annual frequency(MAF) of exceedance with a certain *EDP* or *PO*, thus, allowing for a direct redesign of the structure.

Assuming a roof drift at yield to be 0.55% of the total height and estimating initially the parameters $\Gamma_1 = 1.30$ and $a_1 = 0.88$, the equivalent yield displacement of the SDOF system is computed: $D_y^* = \dfrac{D_y}{\Gamma_1}$.

In order to proceed further, the Hazard Curve of Jan Jose, California, and the corresponding Hazard Spectra were used.
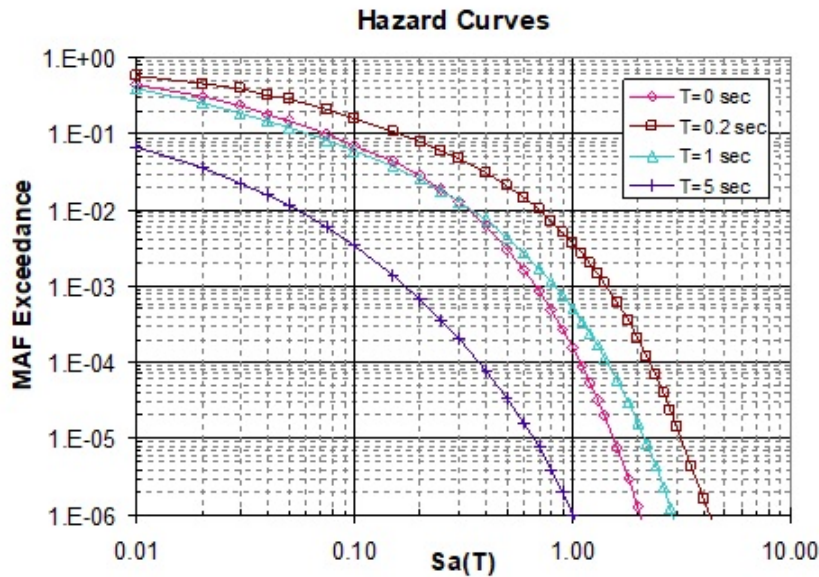
Figure 2.2: Seismic hazard for the San Jose site, California(Aschheim)
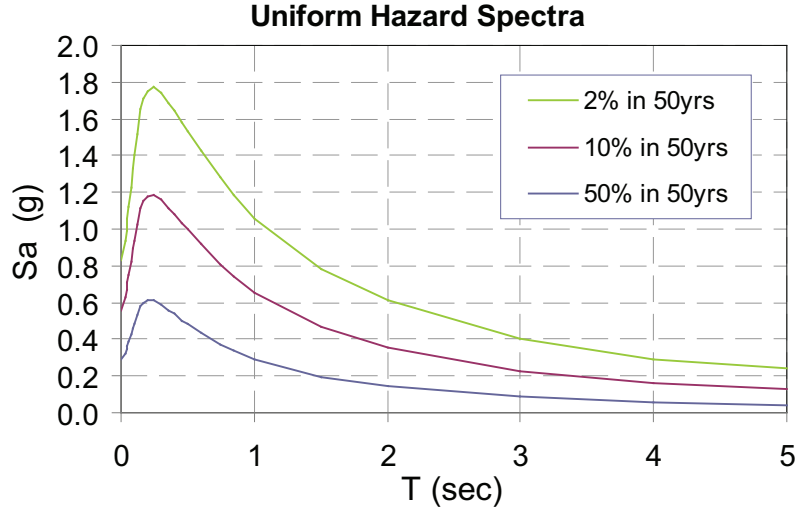
Figure 2.3: Uniform hazard spectra, San Jose(Aschheim)

The corresponding Yield Point Spectrum for the 2/50 level hazard was developed and shown below. With this at hand, the normalized strength coefficient, C_y^* of the SDOF system is calculated, with parameters D_y^*, μ^* known:
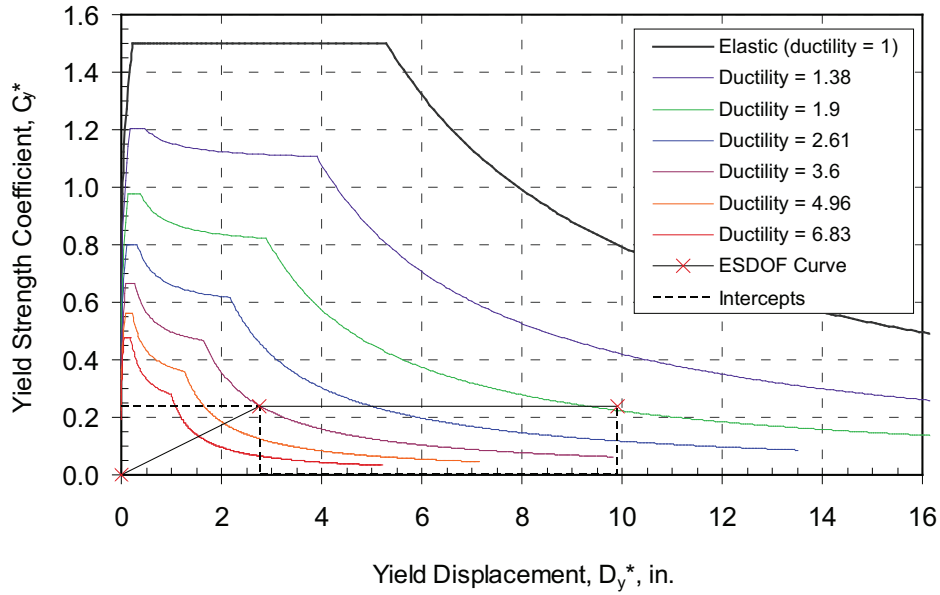
Figure 2.4: Yield Point Spectrum for the 2/50 hazard(Aschheim)

From this point on, the period of the SDOF system and the base shear of the MDOF system can be estimated.

- $T^* = 2\pi\sqrt{\dfrac{D_y^*}{C_y^* \cdot g}} = 1.08 \; sec$

- $V_y = \alpha_1 \cdot C_y^* \dfrac{W}{2} = 1579 \; kips$

Making use of the Equivalent Lateral Force method of ASCE-7 in conjuction with T^*, the lateral force distribution according to the first mode is determined. The Portal Frame Method is then used, with the assumption that inflection points for the columns of the first story occur at 70% of the height, while for the rest of the storys, it occurs at 60%. With these assumptions a moment distribution is calculated for the whole structure and the initial sizing can begin.
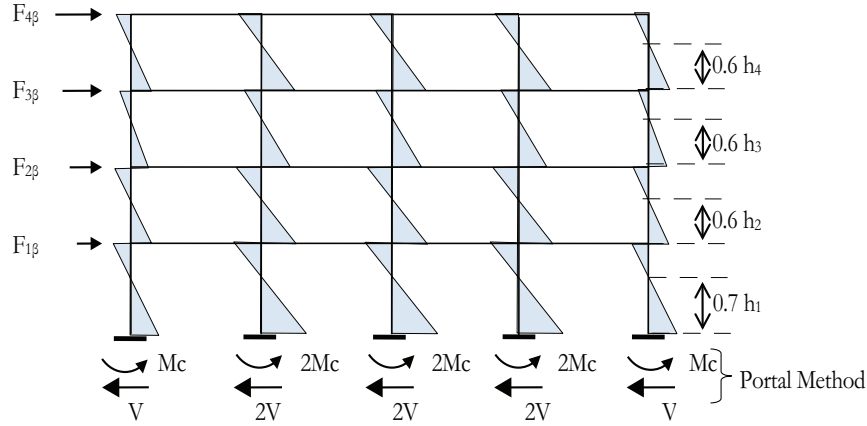
Figure 2.5: Portal Frame Method for determining column and beam moments and shears(Aschheim)

The design pattern was the following:

- External columns with lighter reinforcement than internal columns

- Columns of a certain story had the same external dimensions.

- Beams of a certain story had the same dimensions and the same reinforcement

- Reinforcement splices are placed at midheight of each story

- Column reinforcement is constant at the floor level

The section and reinforcement sizes were based on expected material properties and the beam and column proportioning was carried out using ACI 318 reduction factor. Moreover, for the top steel of the beams, the following ACI 318 requirement was taken into consideration:

$$M_n^+ \geq \frac{1}{2}M_n^-$$

At join level, the following requirement had to be also satisfied:

$$\sum M_{n,col} \geq \frac{6}{5}\sum M_{n,bm}$$

The overall reinforcement sizing pattern, along with beam and column reinforcement tables are presented below, as estimated by prof. Aschheim.

Table 2. Mathematical Solution for Beam Sizes and Reinforcing

Level	Required Strengths		Mathematical Solution			
	M_p^- (kip-in)	M_p^+ (kip-in)	b_w (in.)	h (in.)	$A_{s,top}$ (in²)	$A_{s,bot}$ (in²)
4	5947	2974	12.92	21.54	5.66	2.00
3	19051	9526	18.43	30.72	11.96	5.07
2	27864	13932	20.77	34.62	15.34	6.67
1	30974	15487	21.43	35.72	16.38	7.48

Table 3. Engineering Design for Beam Sizes and Reinforcing

Level	b_w (in.)	h (in.)	Top Bars	Bottom Bars
4	14	22	(6) No 9	(3) No 8
3	18	32	(12) No 9	(7) No 8
2	24	36	(16) No 9	(9) No 8
1	24	36	(16) No 9	(10) No 8

Table 4: Design of Sections of Intermediate Columns Just Above Floor Levels

Floor	Mc or Mpc	D+0.25L	h	As	Bars	As, provided	P/Agfce	ρ_g, %
Level	k-in	k	in.	in.²		in.²		
4	0	NA	NA	NA	NA	NA	NA	NA
3	15431	78.75	26	23.79	(20) No 10	25.40	1.79%	3.76%
2	23573	163.13	30	29.84	(24) No. 10	30.48	2.79%	3.39%
1	25089	247.50	32	27.70	(24) No. 10	30.48	3.72%	2.98%
Footing	46488	331.88	36	47.73	(36) No. 10	45.72	3.94%	3.53%

Table 5: Design of Sections of Intermediate Columns Just Below Floor Levels

Floor	Mc	D+0.25L	h	As	Bars	As, provided	P/Agfce	ρ_g, %
Level	k-in	k	in.	in.²		in.²		
4	10705	78.75	26	15.25	(20) No 10	25.40	1.79%	3.76%
3	18861	163.13	30	22.61	(20) No 10	25.40	2.79%	2.82%
2	26582	247.50	32	29.83	(24) No. 10	30.48	3.72%	2.98%
1	30665	331.88	36	28.01	(24) No. 10	30.48	3.94%	2.35%
Footing	NA	NA	NA	NA	NA	NA	NA	NA

Table 6: Design of Sections of End Columns Just Above Floor Levels

Floor	Mc or Mpc	D+0.25L	h	As	Bars	As, provided	P/Agfce	ρ_g, %
Level	k-in	k	in.	in.²		in.²		
4	0	NA	NA	NA	NA	NA	NA	NA
3	9602	78.75	26	13.36	(12) No 10	15.24	1.79%	2.25%
2	15047	163.13	30	16.97	(16) No. 10	20.32	2.79%	2.26%
1	16726	247.50	32	16.17	(16) No. 10	20.32	3.72%	1.98%
Footing	23244	331.88	36	19.23	(16) No. 10	20.32	3.94%	1.57%

Table 7: Design of Sections of End Columns Just Below Floor Levels

Floor	Mc	D+0.25L	h	As	Bars	As, provided	P/Agfce	ρ_g, %
Level	k-in	k	in.	in.^{2}		in.^{2}		
4	7137	78.75	26	9.23	(12) No 10	15.24	1.79%	2.25%
3	13260	163.13	30	14.41	(12) No 10	15.24	2.79%	1.69%
2	18390	247.50	32	18.40	(16) No. 10	20.32	3.72%	1.98%
1	20443	331.88	36	16.01	(16) No. 10	20.32	3.94%	1.57%
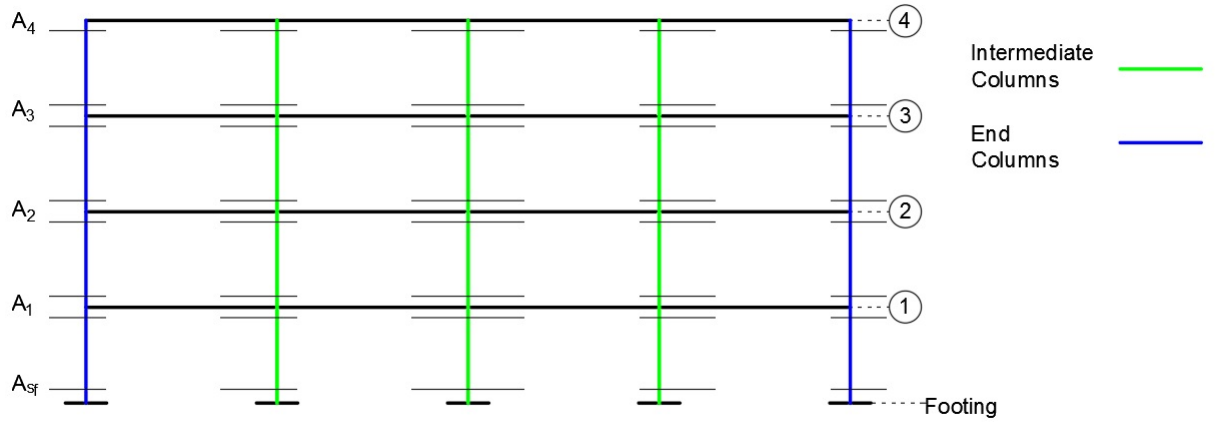
Figure 2.6: Reinforcement pattern

The preliminary Design was modeled in SeismoStruct by prof.Aschheim using fiber elements with specified plastic hinge length at the end. The material constitutive law for concrete and steel fibers allowed for intelastic response. For this evaluation, only non-linear static analysis was conducted, according to a lateral force distribution according to the first eigenshape:

	$F_{1st}(Kips)$
4	639
3	443
2	276
1	118

Figure 2.7: Capacity curve, Seismostruct

The period of the uncracked structure, determined from eigenvalue analysis, is $T_1 = 0.787 sec$, while the period associated with the secant stiffness was estimated by the following formula:
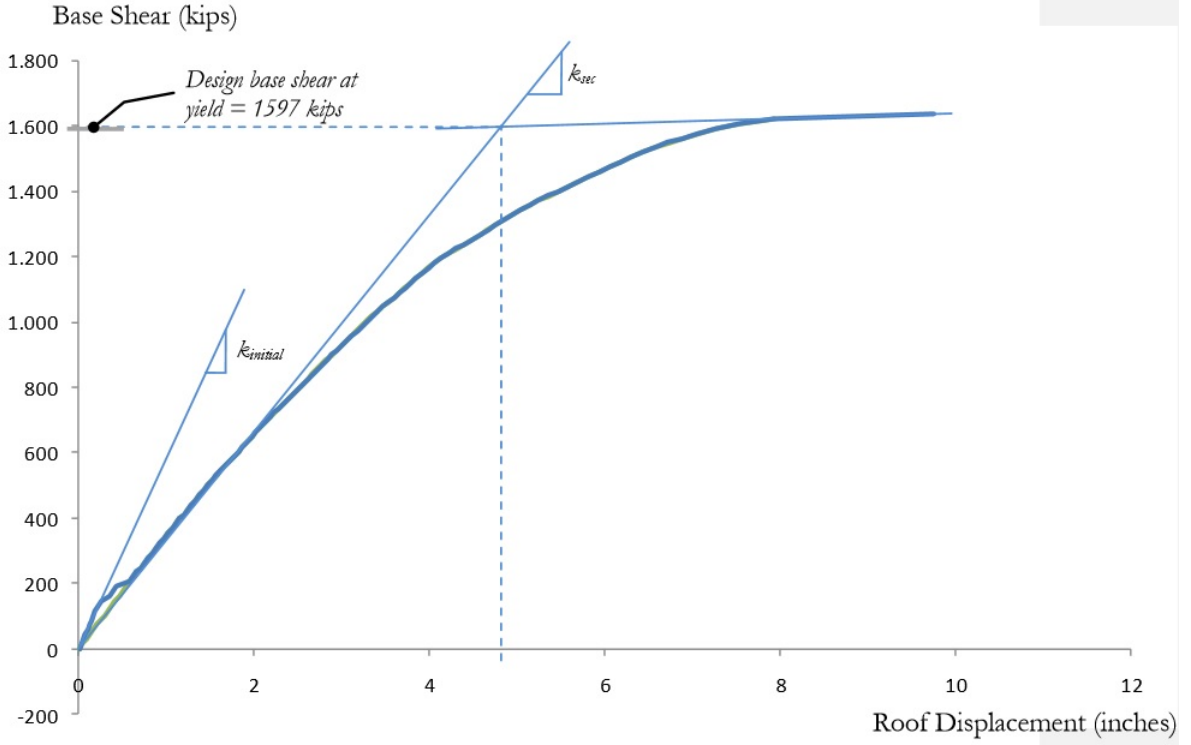
$$T_{sec} = T_1 \cdot = \sqrt{\frac{K_{init}}{K_{sec}}} = 0.787 \cdot \sqrt{\frac{590}{330}} = 1.05 \ sec \tag{2.1}$$

which compares well to the $1.08 \ sec$ of the SDOF estimated from the Yield Point Spectrum. Moreover, the maximum base shear $V_b = 1597 \ kips$ also compares well with the value of $1579 \ kips$ that was estimated based on the initial assumptions. As for the corresponding parameters of the equivalent SDOF system, from the Seismostruct model $\Gamma_1^s = 1.36$ and $\alpha_1 = 0.63$. Thus, $C_y* = C_y/\alpha_1 = 0.336$ and $D_y* = D_y/\Gamma_1 = 3.53 \ in$. From the Yield Point Spectrum, the new yield point, as shown below, on the $\mu = 2.65$ contour, which is lower than the ductility objective ($\mu_{obj} = 3.6$). The peak roof displacement is estimated as $D_y \cdot \mu = 4.8 \cdot 2.65 = 12.7 \in$, where $D_y = 4.8 \ in$ the roof yield displacement according to the non-linear static analysis in Seismostruct. This also is lower than the peak roof displacement limit derived from the initial assumptions, which was $D_u^{lim} = 19.1 \ in$.
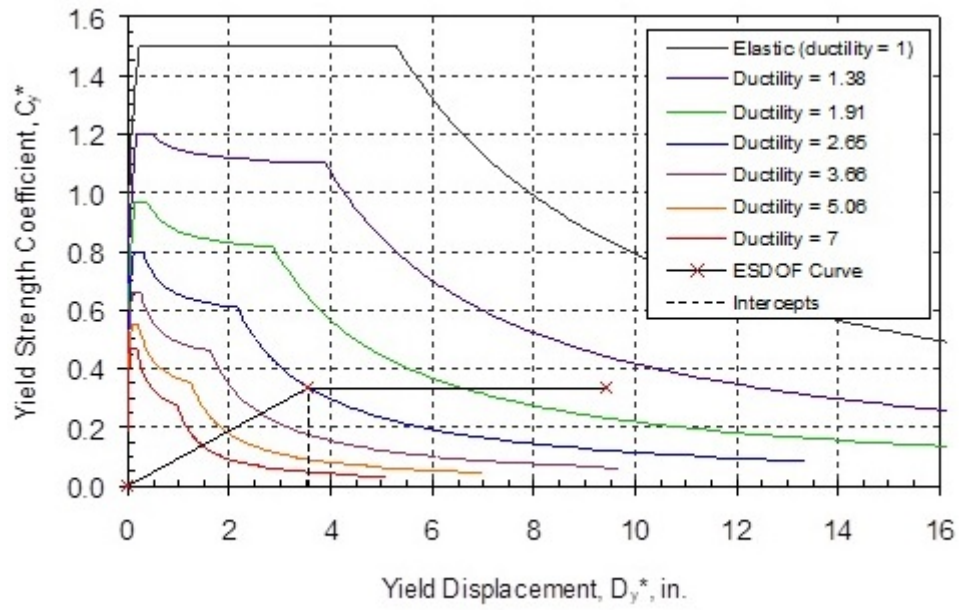
Figure 2.8: Updated yield displacement

All in all, the resulting design complies with the objective limits on ductilily and interstory drift, upon which the initial assumptions for the design were based.

Chapter 3

Finite Element Modeling in OpenSees

3.1   General Concerns

As stated in the introduction, the structure will be simulated using two different models: one where the inelastic behaviour of beam-column element is concetrated at its ends, while the interim remains elastic, and another where, in contrast, damage is allowed to spread over the element lenght. The latter is the case of the fiber - distributed - plasticity beam-column elements. A more accurate representation of the behaviour prior to reaching the maximum base shear is generally expected from the fiber model, where cracking of the unconfined cover concrete is taken into account in section level and properly , along with the gradual plastification of distinct fibers or "layers" at cross-section level. By strategically picking interior integration (Gauss) points -which are the cross-sections- the element state determination is carried out in a *weighted* manner by the (weighted) sum of specific properties from these points.

Moreover, within the context of distributed plasticity elements, changes in the plastic moment strength of a section due to changes in the element axial force is adjusted automatically, since it is the specified constitutive law specified for each fiber that controls the section, element and, after all, structural behaviour. This feature is important in cases where non-negligible variations in the column axial forces occur, such as the case of a high-rise building of small span during ground motion.

On the other hand, lumped plasticity elements confine the plastification -usually- at the two end nodes of the element and the aspect here is the user-defined force-displacement curve at section level. That is, phenomenological models like moment-curvature law in the simplest case or more complex ones that take into consideration interactions between the stress resultants (e.g Bouc-Wen hysteretic model). Those models have significantly lower demands as far as computation cost is concerned and, in contrast with the fiber elements, they tend to be stable even if the global equilibrium path (capacity curve) exhibits softening behaviour.
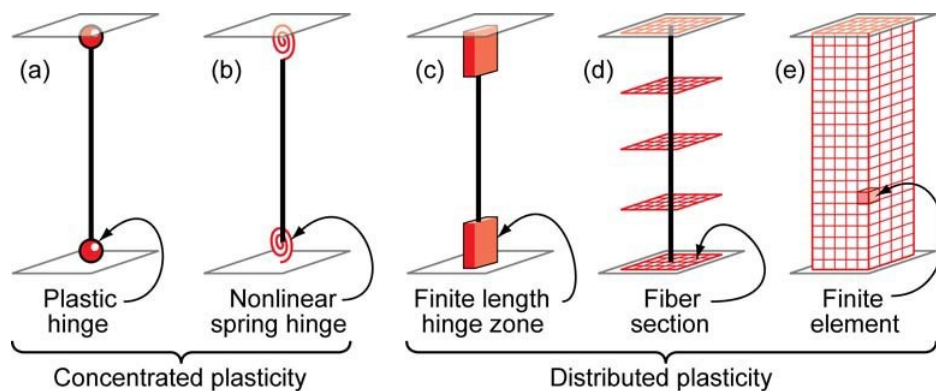
Figure 3.1: Beam-Column Element Models-courtesy of NIST 10-917-5- (2010). (from M.Aschheim)

Since IDA is a computationally costly analysis and convergence issues are expected in the fiber model as non-linear behaviour increases, our end motive is to take advantage of the accurate representation of the fiber models equilibrium path prior to reaching its maximum base shear and calibrate the lumped model accordingly. Up until that point, if the modelization is a adequate, both models should yield approximately the same maximum base shear.

A presentation of the two approaches is presented below, where focus will be given to the different elements used.

3.2   Lumped plasticity model

As stated before, in the lumped plasticity approach, discrete nonlinear moment-curvature or moment-rotation springs are placed at the ends of each element. There are various ways for this approach, as can be seen from Fig 3.1. In (a) and (b) for example, zero length elements are placed at the ends of the beam-column element and an elasto/rigid-perfectly plastic and non-linear law is specified respectively for the moment-rotation/curvature. In contrast, in model(c) the hinges have finite length, thus allowing for a more accurate representation of the displacements within this context, where plastification is expected mainly at the element ends. The latter approach is followed in this work.

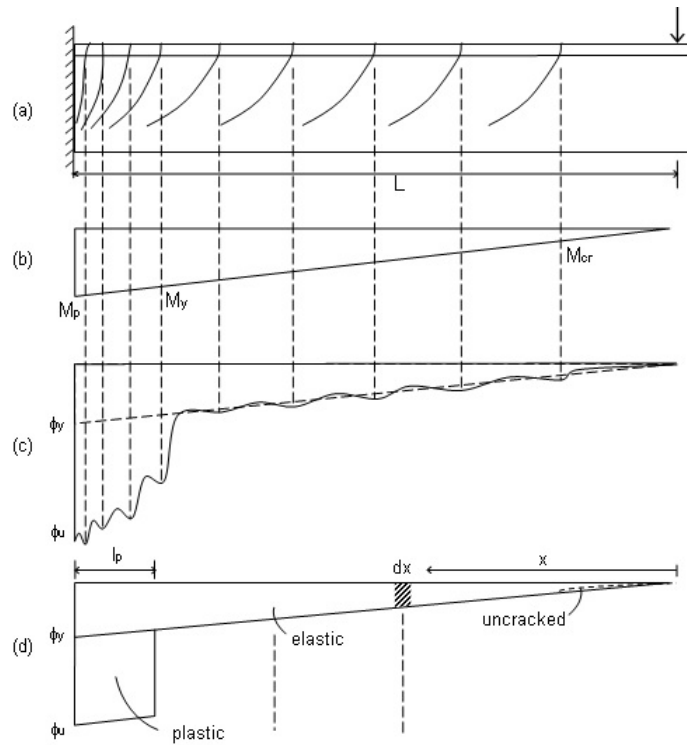Figure 3.2: Curvature distribution in a cantilever. Plastification speads within a specified length from the end (from M.Aschheim).

The specified hinge moment-curvature law is based on the Generalized Load-Displacemement(backbone) curve which can represent beam,column,join or wall component response and is based on ASCE/SEI-41 (2013).
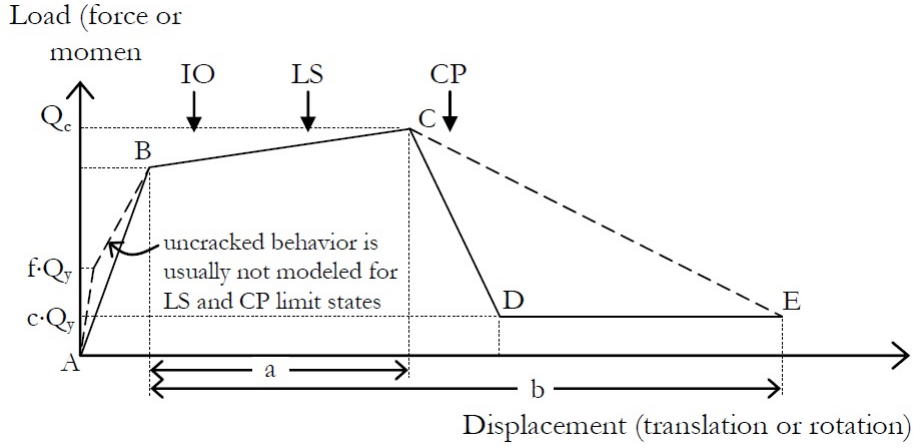
Figure 3.3: Generalized Load-Displacement curve, ASCE-SEI-41(from M.Aschheim)

.

Input is given in terms of moment (for load) and curvature (for displacement). In our case, we chose the isotropic hardening for beams and columns to be 0.001 and 0.01 respectively. Effectively, this means -especially for beams- that $Q_y \rightarrow M_y = M_p \rightarrow Q_p$. Parameters a and b control the capping(point **C**) and ultimate (point **E**) curvature respectively and can be determined based on modeling and acceptance criteria from ASCE SEI-41. Parameter f can be specified in order to introduce an initial increased flexural stiffness due to uncracked response, generally accounting for $0.2 \div 0.3$, but is ignored here. Instead, as will be discussed later on, calibration will be carried out on a global level, based on the fiber model response. Finally, the parameter c controls the residual flexural strength and usually accounts for ≈ 0.2. Softening of reinforced concrete sections is to be expected. In the present work, point D is bypassed and a smoother softening segment is specified, that is, $C \rightarrow E$.

3.2.1 Beams

The beam sections were designed in order to satisfy the following condition:

$$M_P^+ = \frac{1}{2} \cdot M_P^-$$

This stems from the fact that under gravity loads, the moment diagram is symmetric, with the top flanges at the ends in tension. Lateral (cyclic) loads due to earthquake however cause beams to develop tension at the top flange of one end and compression at the respective flange of the other end, thus relieving the latter and intensify the former.
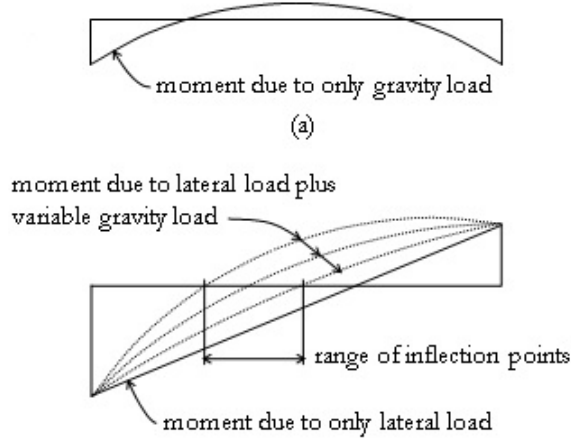
Figure 3.4: Beam under gravity and combined gravity-lateral loads(from M.Aschheim)

.

For this reason, the moment-curvature law will be unsymmetric for the case of beam end hinges. The negative and positive moments are calculated according to the following formulas:

$$M_P^+ = \frac{2}{3} M_{Pb}(1 - \frac{h_{col}}{L}) \quad \text{and} \quad M_P^- = \frac{4}{3} M_{Pb}(1 - \frac{h_{col}}{L}) = 2M_P^+$$

where M_{Pb} is a theoretical uniform(common) plastic flexural strength, used to derive the collapse load factor by the kinematic method. The above expressions ensure that the internal work produced at the node after imposing the design constraint $M_P^+ = 1/2M_P^-$ is still equal to $2M_{Pb}\theta$. These values are shown in the sizing tables provided in the previous chapter.

As for the yield curvatures, these are derived from the from the following estimates:

$$\phi_y^- = \frac{1.8\epsilon_y}{h_b} \quad \text{and} \quad \phi_y^+ = \frac{1.4\epsilon_y}{h_b}$$

With the yield curvatures at hand, and by assuming a plastic hinge length of $\approx 2 \cdot d_b$, where d_b is the static depth of the beam, the yield rotation within the range of the hinge length can be estimated as:

$$\theta_y^- = \phi_y^- \cdot d_b \quad \text{and} \quad \theta_y^+ = \phi_y^+ \cdot d_b$$

Anchorage slip

The effect of reinforcement slip that is anchored within the adjoining member (e.g. joint or wall) is also considered in the present hinge model. The anchorage slip due to strains, along with some deformation that occurs on the compression face, introduces a concetrated rotation at the beam end. In the present work, this rotation is not expressed in terms of loading history, but is added as an additional increment to θ_y, thus defining point B(M_P, θ_B) in Figure 3.3, where $\theta_B = \theta_y + \theta_{slip}$.

The slip rotation can be estimated from the following expression:

$$\theta_{slip} = \frac{\phi y d_b f_y}{108\sqrt{f_c'}}$$

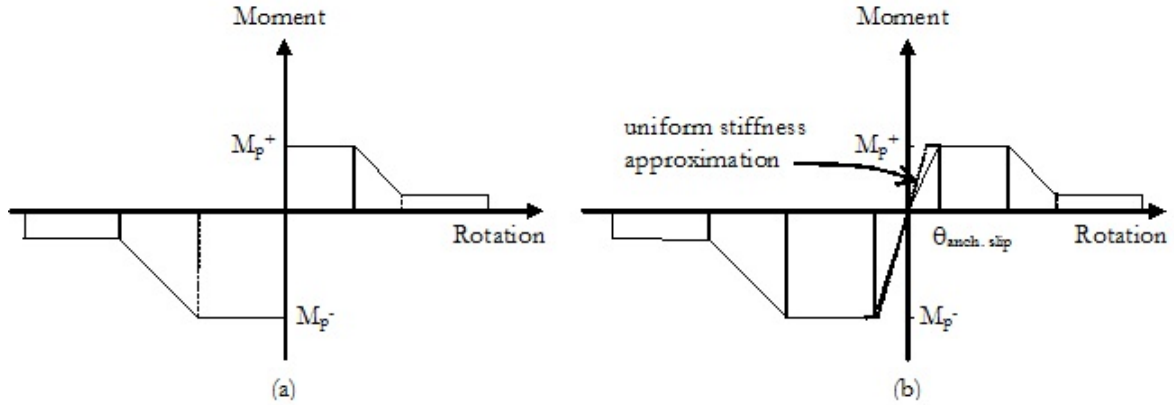Rotation due to anchorage slip will only be considered for beams.

Figure 3.5: (a) Rigid-plastic and (b) Elasto-plastic with slip included (from M.Aschheim)
.

Points C and E in Figure 3.3 can be determined from ASCE SEI-41, Table 10-7 (2013), which defines the modeling and acceptance criteria for beam plastic hinges.

Table 17.2 Modeling and acceptance criteria for beam plastic hinges (excerpted from ASCE SEI 41 Table 10-7 (2013))

Condition		Modeling parameters			Acceptance Criteria		
$\dfrac{\rho - \rho'}{\rho_{bal}}$	$\dfrac{V}{b_w d \sqrt{f_c'}}$	Plastic rotation angle, radians		Residual strength ratio	Acceptable plastic rotation angle, radians		
		a	b	c	Performance Level		
					IO	LS	CP
≤ 0.0	≤ 3 (0.25)	0.025	0.05	0.2	0.010	0.025	0.050
≤ 0.0	≥ 6 (0.50)	0.02	0.04	0.2	0.005	0.020	0.040
≥ 0.5	≤ 3 (0.25)	0.02	0.03	0.2	0.005	0.020	0.030
≥ 0.5	≥ 6 (0.50)	0.015	0.02	0.2	0.005	0.015	0.020

Figure 3.6: Modeling parameters, ASCE SEI-41(from M.Aschheim)

Below the modeling parameters a and b are presented in a tabulated form.

Table 3.1: Modeling parameters for negative and positive moment (BEAMS)

Story	M_P^+		M_P^-	
-	a	b	a	b
1	0.0228	0.0457	0.0190	0.0257
2	0.0233	0.0467	0.0197	0.0267
3	0.0231	0.0462	0.0193	0.0262
4	0.0250	0.0500	0.0202	0.0310

3.2.2 Columns

For the columns, anchorage slim is assumed neglibible and the yield curvature is determined by the following formula:

$$\phi_y = (1.8 - 1.3\frac{P}{A_g f_c'} + 9(\rho_g - 0.025))\frac{\epsilon_y}{d}$$

where A_g is the gross sectional area of the column, ϵ_y is the yield strain of the steel rebars and d the static depth of the column.Nominal material values are used for concrete.
The above equation, derived by prof.Aschheim, is a reasonable fit to moment-curvature data where longitudinal steel ratio ρ_g is also included as a possible parameter that affects column flexural stiffness, along with the axial load ratio $P/A_g f_c'$.
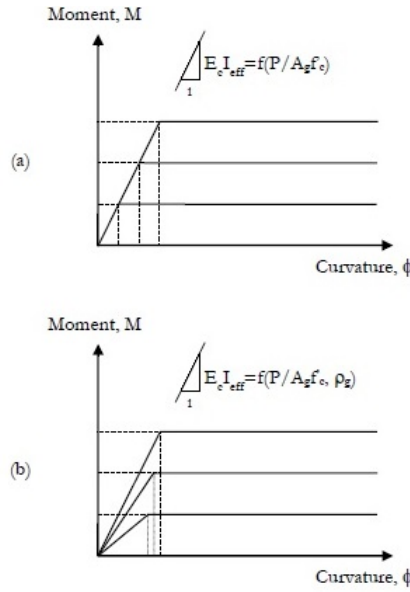

Figure 3.7: (a) Flexural stiffness dependence only on axial load ratio and (b) including reinforcement steel ratio (from M.Aschheim)

.

Figure 3.8 illustrates the dependency of flexural stiffness and yield curvature on the longitudinal steel ratio.
The modeling parameters and acceptance criteria for the column plastic hinges of rectangular cross-section are provided from Table 10-8 of ASCE SEI 41. Potential change in modeling parameters a, b should be expected in general, however, in this case these parameters were almost the same for each column.

Table 3.2: Modeling parameters for columns, below and above floor level

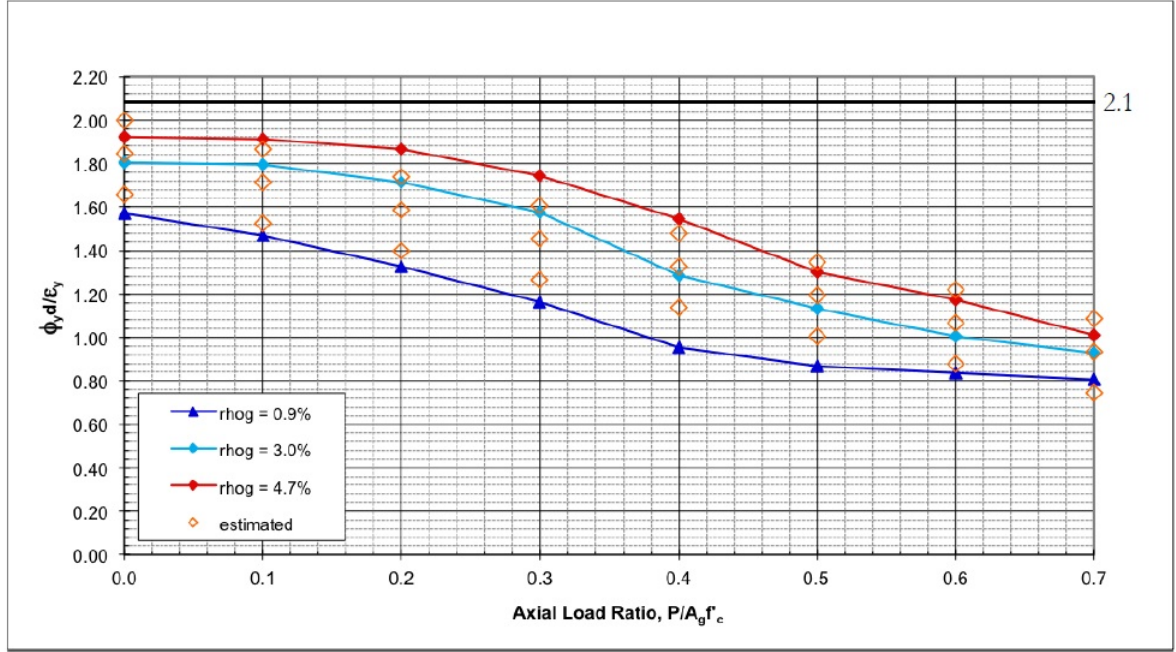| *Story*	Below		Above	
-	a	b	a	b
1	0.030	0.044	0.030	0.044
2	0.030	0.044	0.030	0.044
3	0.030	0.044	0.030	0.044
4	0.030	0.054	0.030	0.044

Figure 3.8: Fits on moment-curvature history data, showcasing dependency on ρ_g (from M.Aschheim)

.

Condition			Modeling parameters*			Acceptance Criteria*		
$P/(A_g f_c')$‡	$\rho_v = A_v/(b_w s)$	$\dfrac{V}{b_w d \sqrt{f'_c}}$ #	Plastic rotation angle, radians		Residual strength ratio	Acceptable plastic rotation angle, radians		
			a	b	c	Performance Level		
						IO	LS	CP
Condition i. $V_e/\phi V_n \le 0.8$ †								
≤ 0.1	≥ 0.006	NA	0.035	0.060	0.2	0.005	0.045	0.060
≥ 0.6	≥ 0.006	NA	0.010	0.010	0.0	0.003	0.009	0.010
≤ 0.1	=0.0036 §	NA	0.030 §	0.044 §	0.2	0.005	0.034	0.044
≥ 0.6	=0.0036 §	NA	0.007 §	0.007 §	0.0	0.002	0.006	0.007
Condition ii. $0.8 \le V_e/\phi V_n \le 1.0$ †								
≤ 0.1	≥ 0.006	≤ 3 (0.25)	0.032	0.060	0.2	0.005	0.045	0.060
≤ 0.1	≥ 0.006	≥ 6 (0.50)	0.025	0.060	0.2	0.005	0.045	0.060
≥ 0.6	≥ 0.006	≤ 3 (0.25)	0.010	0.010	0.0	0.003	0.009	0.010
≥ 0.6	≥ 0.006	≥ 6 (0.50)	0.008	0.008	0.0	0.003	0.007	0.008
≤ 0.1	=0.0036 §	≤ 3 (0.25)	0.023 §	0.039 §	0.2	0.005	0.030	0.039
≤ 0.1	=0.0036 §	≥ 6 (0.50)	0.017 §	0.036 §	0.2	0.005	0.028	0.036
≥ 0.6	=0.0036 §	≤ 3 (0.25)	0.007 §	0.007 §	0.0	0.003	0.006	0.007
≥ 0.6	=0.0036 §	≥ 6 (0.50)	0.005 §	0.005 §	0.0	0.002	0.004	0.005

Figure 3.9: Modeling parameters and acceptance criteria for column plastic hinges of rectangular cross-section, ASCE SEI 41 (from M.Aschheim)

.

3.2.3   Element and structural model

The Lumped model makes use of the *beamWithHinges element* of OpenSees for both beams and columns. The hinges at the ends are defined by assigning the *Pinching4 material* law as a prescribed moment-rotation response to them, which is capable of exhibiting pinching and degradation under cyclic loading[1].
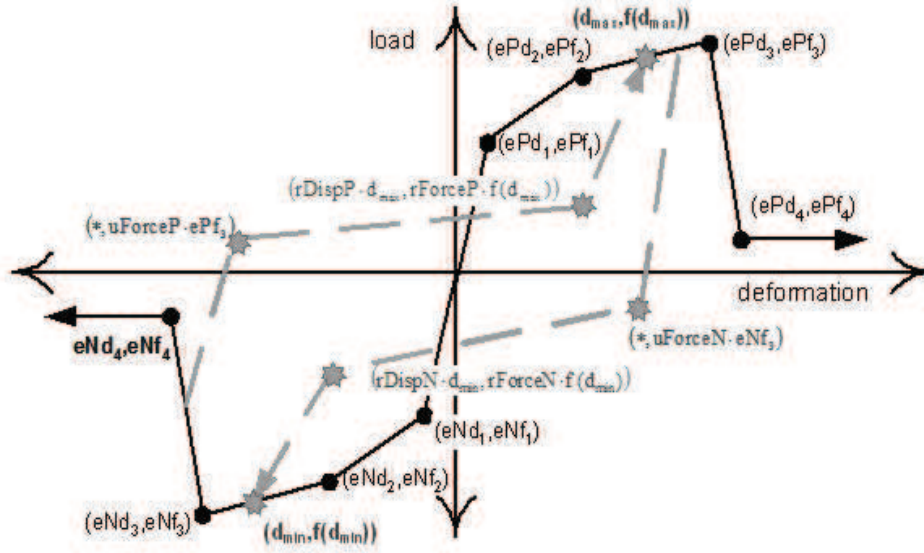

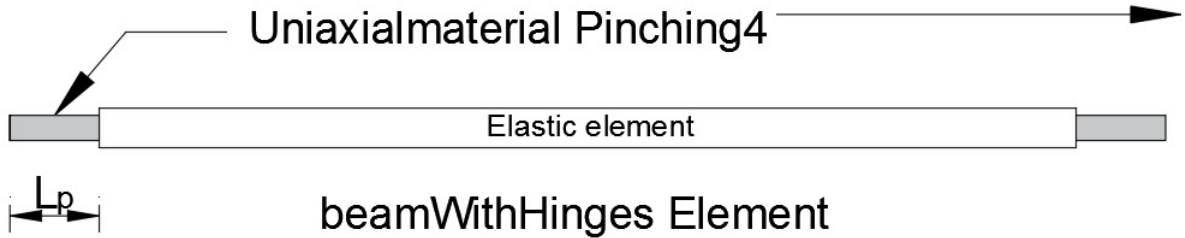
Figure 3.10: Pinching4 uniaxial law, OpenSeesWiki

.

Figure 3.11: Typical beamWithHinges element model

It is worth pointing that although this element is used mostly as an effort to reconcile the lumped and fiber element by specifying a finite length zone at the ends where one or even two integration points are places (according to the integration method), however, in the present work, in order for the *pinching4* material to be compatible and give reasonable results, the plastic hinge length was specified as 0.001% of the element length, which effectively makes it concetrated.

As for the structural model, a leaning column was placed next to the rightmost columns in order to account for mass that is not tributary to the frame and, subsequently, possible $\Pi - \Delta$ effects. The geometric properties of the leaning column are determined from the sum of all interior columns of the half building. Moreover, the displacement compatibility

---

[1]http://opensees.berkeley.edu/wiki/index.php/Pinching4_Material

with the frame is enforced with the *equalDOF* command. This command is also used to impose a diaphragm constraint for each story. It should be emphasized here that whenever a leaning column is used in a simulation, it should be connected either by using semi-rigid truss elements or the equalDOF command **with the adjacent frame column**. Otherwise, gravity loads will induce parasitic axial forces to the beams.
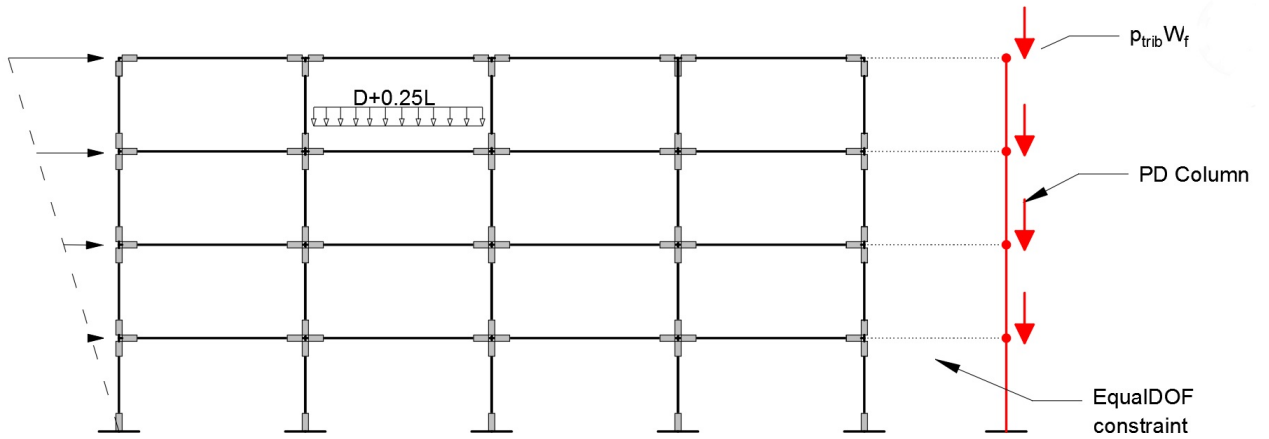

Figure 3.12: Frame model

3.3 Distributed Plasticity Model

For the this model, the flexibility approach is adopted and each member is discretized with only one element. In each element five integration points are used and the corresponding section also discretized into fibers.

3.3.1 Material laws

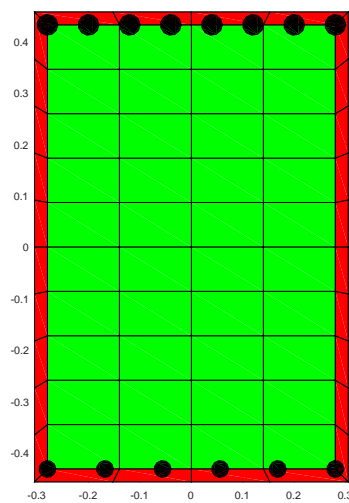A typical fiber section can be seen in the following picture.

Figure 3.13: Typical cross-section

Each of the three materials, that is, unconfined (red), confined (green) concrete and steel(black) is assigned with its respective constitutive law from the material library of OpenSees.

Unconfined Concrete

For the unconfined part, the *uniaxialMaterial Concrete01*[2] is used. This material has zero tensile strength.
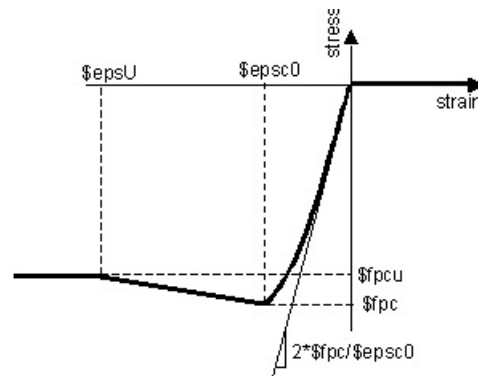

Figure 3.14: Concrete01 material, OpenSeesWiki

Confined Core

For the confined core, Chang & Mander's (1994) concrete model[3] is used, which is the *uniaxialMaterial Concrete07*[4] in Opensees.
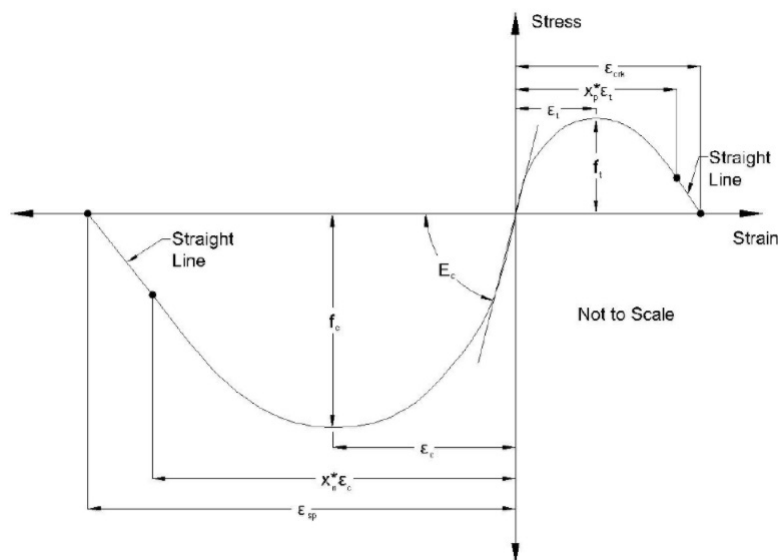

Figure 3.15: Concrete07 material, OpenSeesWiki

---

[2]http://opensees.berkeley.edu/wiki/index.php/Concrete01_Material_–_Zero_Tensile_Strength

[3]Chang, G.A., and Mander, J.B., (1994) "Seismic Energy Based Fatigue Damage Ananlysis of Bridge Columns:Part 1 – Evaluation of Seismic Capacity," NCEER Technical Report No. NCEER-94-0006 State University of New York, Buffalo, N.Y.

[4]http://opensees.berkeley.edu/wiki/index.php/Concrete07_%E2%80%93_Chang_%26_Mander%E2%80%99s_1994_Concrete_Model

Steel

Reinforcement steel is modeled after the *uniaxialMaterial Hysteretic*[5]
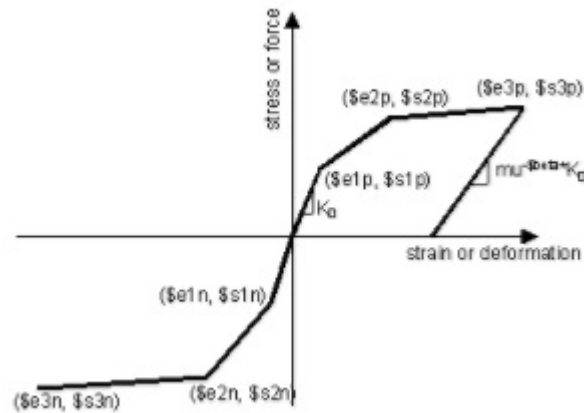

Figure 3.16: Hysteretic material, OpenSeesWiki

Performing a curvature-controlled analysis of increasing (cyclic) amplitude of a first story beam cross-section, yields the following graph:
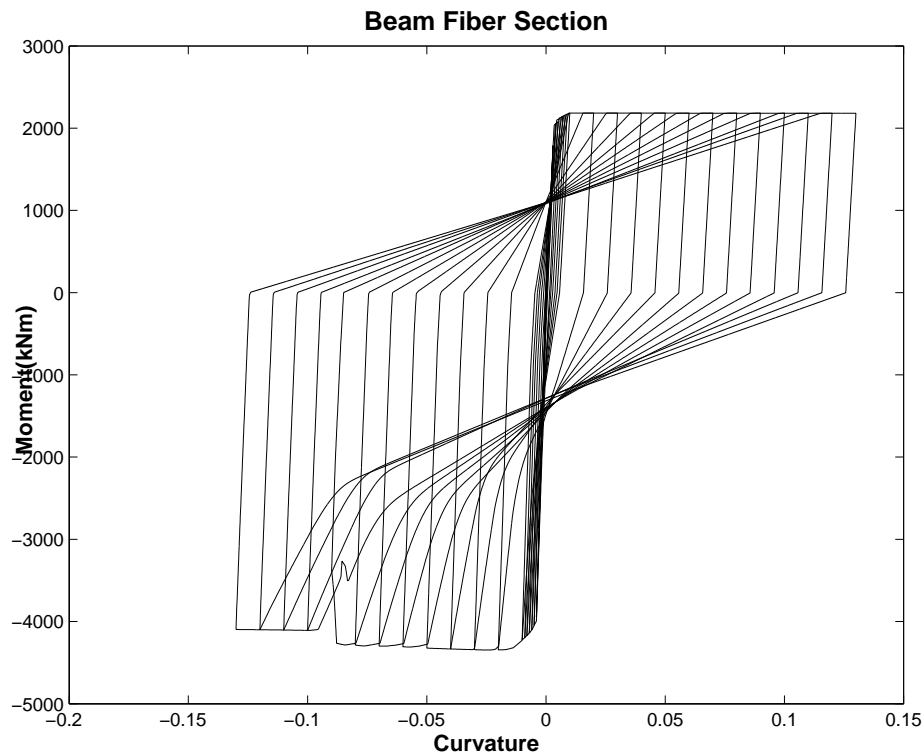

Figure 3.17: 1st story beam cross-section response under cycling loading history

where it can be seen that the positive plastic moment strength is half its negative counterpart.

---

[5]http://opensees.berkeley.edu/wiki/index.php/Hysteretic_Material

3.3.2 Fiber elements

Beams

For each beam member one force-based finite element is used with five integration points. The integration method used is Gauss-Lobatto rule, where two integration points are placed at the element ends. This formulation is represented in Opensees by the *nonlinearBeamColumn* element.
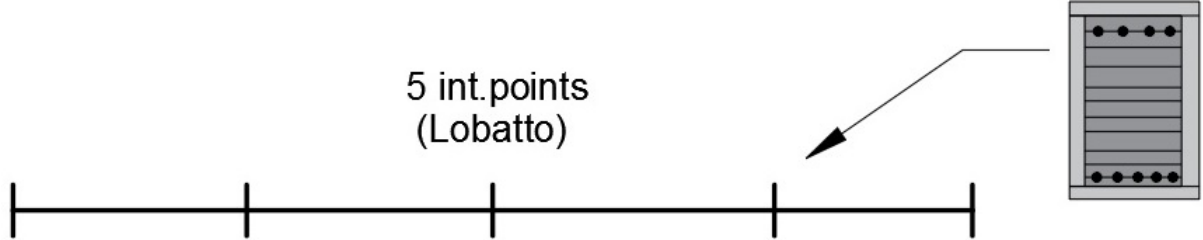

Figure 3.18: Force-based beam-column element (Lobatto)

Columns

For columns, the *forceBeamColumn* element was used. This is also a flexibility-based formulation, with the addition that it allows assigning different cross-section tags, thus sections, at each integration point. This is particularly usefull for this case since the reinforcement configuration between top and bottom sections of each column is different. Another advantage of this approach is that it allows the user to set different integration rules (e.g. Gauss-Legendre/Lobatto) and,by this, it can be easily reduced to the Lobatto case of the *nonlinearBeamColumn* element.
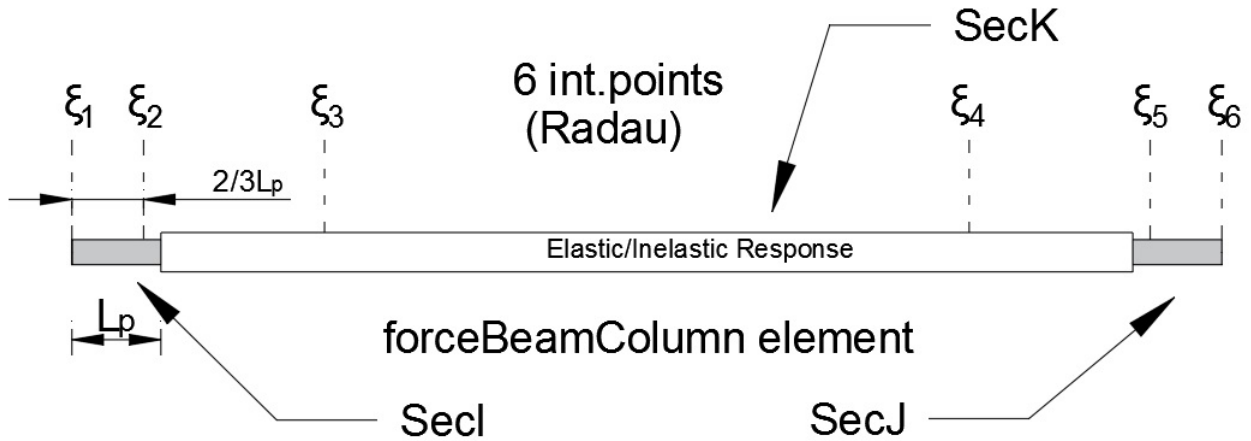

Figure 3.19: Force-based beam column element(Radau)

The Gauss-Radau integration rule was used in this case, where plastic hinge length have to be explicitly specified and then, as can be seen from Fig 3.19, six integration points are placed, with four of them being within the hinge length. Three sections were used along the element length: those specified for the bottom (*above floor level*), for the top (*below floor level*) and since no data was available for the interim, the average steel reinforcement of the aforementioned sections is used as representative of integration points ξ_3 and ξ_4.

3.3.3 Structural Model

Various approaches were examined in this case. In this chapter, only the final model will be presented here, while detailed comments on the rest are left for the next chapter and the discussion of non-linear static analysis results.
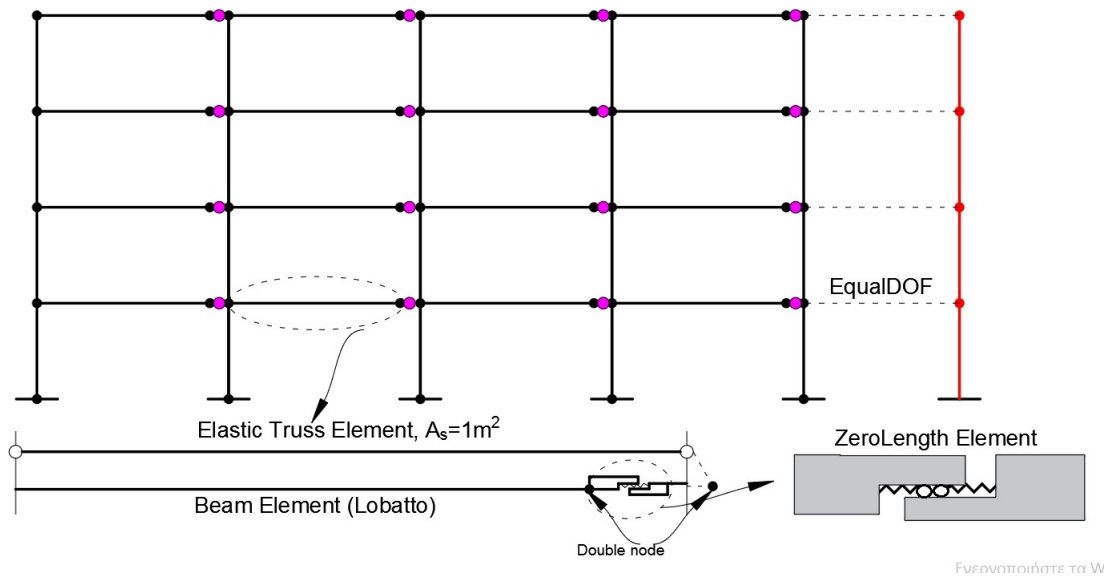

Figure 3.20: Finalized fiber model

When certain fiber RC flexural elements (-typically beams) are designed with significant asymmetry in their reinforcement configuration, imposing *equalDOF* to model the slab effect at each floor will lead to the development of large parasitical axial forces. Thss happens because this particular constraint enforces a zero axial strain condition on the element centerline, which coincides with the floor level. When the section is nonsymmetric or even symmetric but belonging to an RC non-linear element, then during plastification, the neutral axis will shift due to inelastic bending, in order to maintain equilibrium in the section level. Thus, the default-elastic centerline fiber/layer should be allowed to deform. The presence of the *equalDOF* constraint enforces zero axial strain there, resulting in large axial resultants and in a significant change in the response of the structure.

Thus, we have to somehow enforce the slab effect without the use of rigid constraints. To this end, double nodes are placed at the right end of each beam and a *zeroLength* element is defined inbetween. Degrees of freedom 2 and 3 (shear and moment respectively) are retained using *equalDOF* command and continuity in the degree of freedom 1 is restored by placing a very stiff elastic truss element. Figure 3.20 demonstrates the details.

Chapter 4

Non-linear Static Analysis

In this chapter, a detailed overview of the four different approaches of the fiber models will be presented along with their response comparison, inlcuding the lumped model, in non-linear static analysis. The global procedure of solving the system of equation is carried out in a displacement controlled fashion.

4.1 Fiber models

4.1.1 Model 1

Model 1 is the simplest model of all. Each story has its nodes constrained with an *equalDOF* command, in order to impose diaphragm constraint, and tied with the respective leaning column node. Master nodes are the ones in the rightmost column, shown in the figure below.
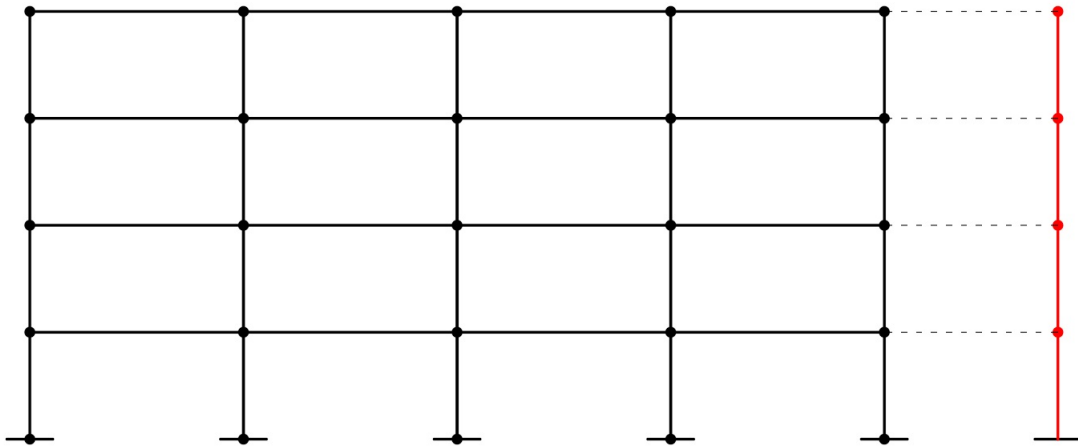

Figure 4.1: Model 1

4.1.2 Model 2

Model 2 is identical to the previous one, with one exception: diaphragm constraint is not imposed at all. The leaning column is again connected to the rightmost frame column via an *equalDOF* command.

4.1.3 Model 3

Model 3 is the one presented in the previous chapter (Figure 3.20). As stated there, double nodes are placed at the right end of each beam. Continuity is retained with

- *zerolength* element and retaining shear and moment DOFs using stiff elastic shear and rotational springs

- placement of an elastic truss element that connects adjacent column nodes in order to simulate the diaphragm constraint

For the axial DOF of the zeroLength element, a spring of low K is used.

4.1.4 Model 4

In this case, some modifications to Model 3 took place. To begin with, truss elements are removed and in their place an *equalDOF* command is used. However, the master nodes this time are the ones in the leftmost column. Then, a *zeroLength* element is again used, with the same properties as before.
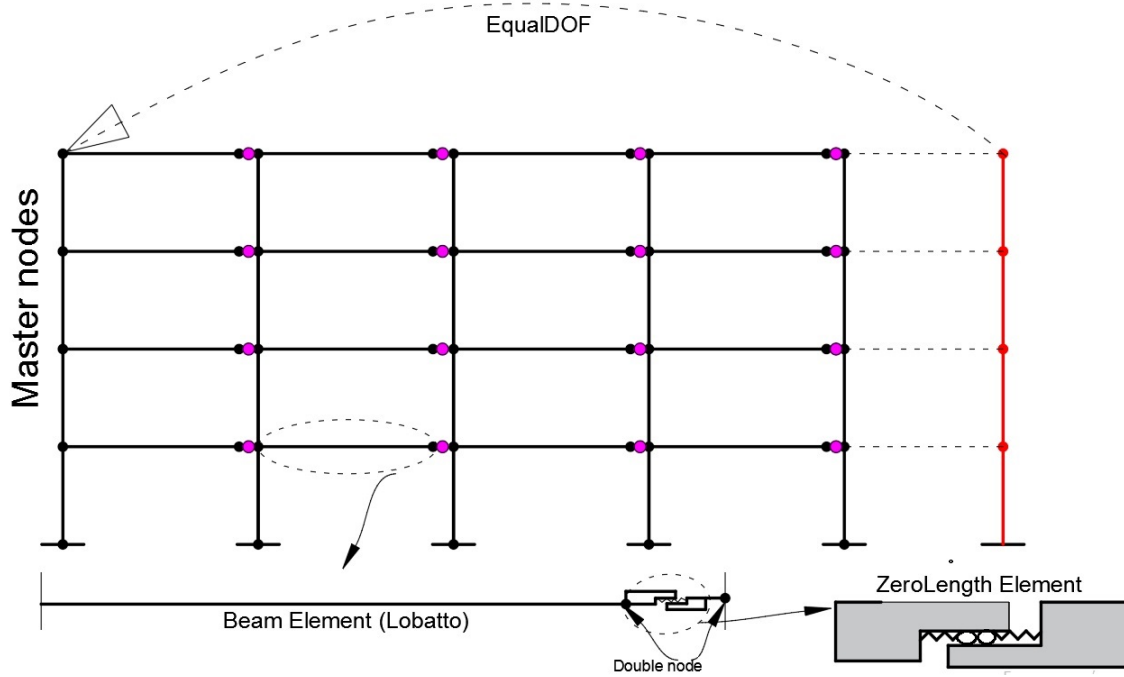

Figure 4.2: Model 4

4.2 Model Response Comparison

As can be seen from Fig.4.3 in the next page, there is significant divergence between the various models. More specifically, the two extreme cases are these of the lumped model response (black) and the Seismostruct with diaphragm constrain active. The latter is significantly stiffer and attain a maximum base shear almost double than that of the lumped. Similarly, model 1 in OpenSees (magenta) exhibits overall the same characteristics. This, as explained before, is a result of the parasitic compressive forces that start developing in the beams as the section layers that should be able to stretch due to flexure are constraint due to *equalDOF* constraint in place.

Moreover, the difference in the maximum base shear of the magenta curve(Model 1) and the Seismostruct model is due to the significant increase in the plastic moment strengths of the beams, as a result of the large parasitic axial forces. Also evident is their lower system ductility, which was expected.

Models 3 and 4, which are represented by the blue and dotted green curve are identical, yielding a maximum base shear of $V_b = 1660 kips$. The period and the drift corresponding to the maximum shear are $T = 0.97 sec$ and $d_u = 0.0254$. However, the execution time of Model 3 where elastic trusses were used for the diaphragm required only 187 seconds, while analysis of Model 4 lasted 343 seconds.

The peak roof displacement is $D_u = 54\ ft \cdot 0.0254 \approx 16.5\ in$ while the respective peak roof displacements from Chapter 1 are $12.7\ in$ from the Seismostruct analysis and
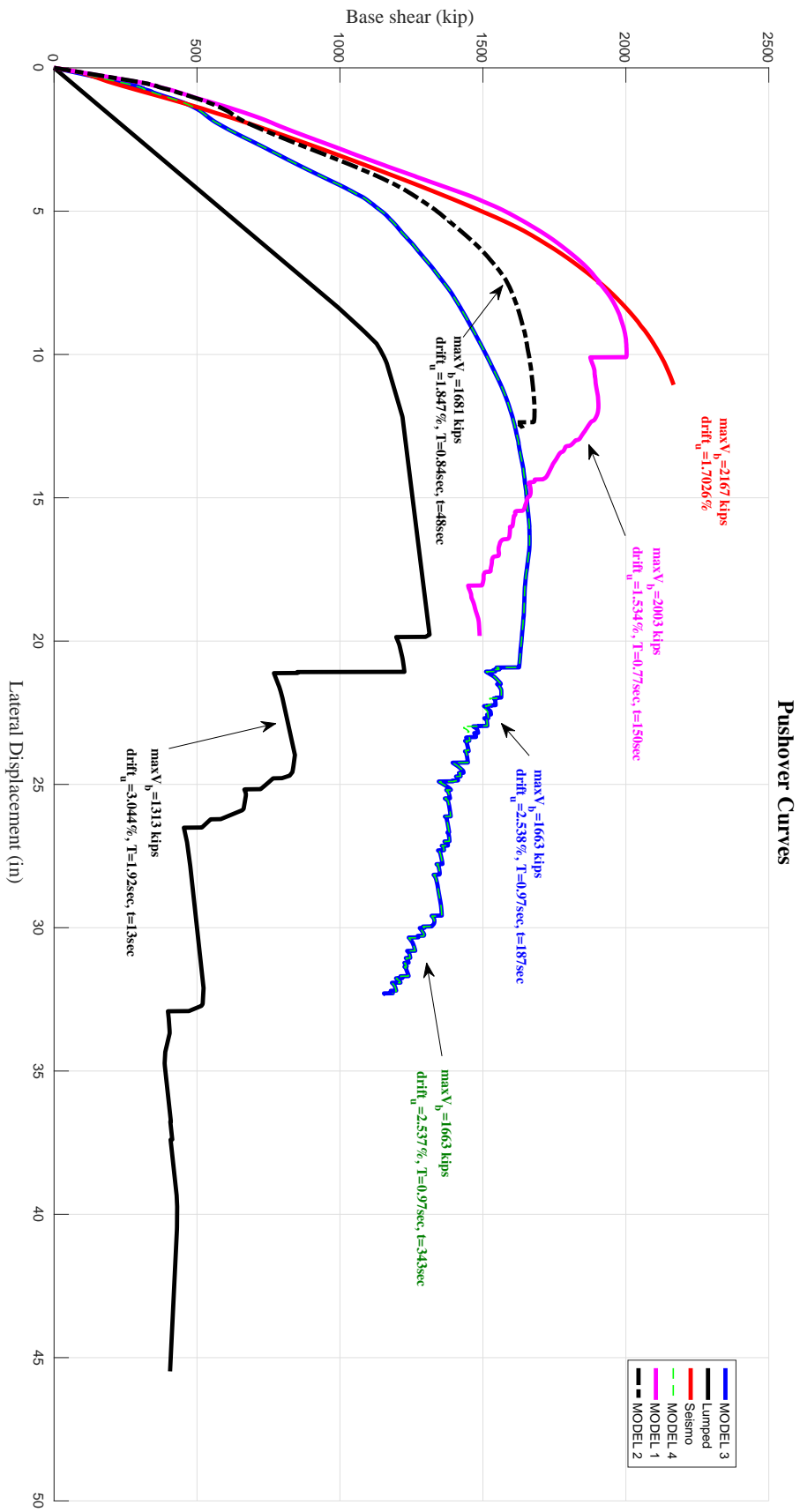
Figure 4.3: Non-linear static pushover analysis comparison

19.1 in from the initial estimations. The maximum base shears compare well, while there is a significant difference in the periods, with the period related to the uncracked stiffness of the Seismostruct model being 0.787 sec compared to that of Models 3 and 4, which are considered as "accurate" amongst the four.

As for Model 2 (dotted black), the analysis yields the same maximum base shear, which was expected since no equalDOF commands were imposed. However, the algorith could not converge past this point, and the analysis stopped. This is probably due to the excessive increase in degrees of freedom for this case, or, alternatively, restricting certain degrees of freedom by imposing an equalDOF command in the other models reduces significantly the unknowns of the linear system, making it more easy to converge.

4.3   Lumped plasticity model refinement

The purpose of having separate fiber models was to capture the pre-capping response accurately, by deciding which of those responses seemed more realistic and consistent. A final modification is applied to Model 3, where the shear and rotational elastic springs defined as the zerolength elements properties with the purpose to ensure continuity are removed and, instead, an equalDOF command is defined for the double nodes, retaining the corresponding (shear and rotational) degrees of freedom. This lead to an overall increase in the execution time of Model 3, however, it lowered its period by 10 sec. The period associated with the final fiber model is $T = 0.87\ sec$.

For the refinement of the lumped model, in order to approach the fiber one in terms of pre-capping response, moment curvature analysis to all fiber sections was performed, taking into account the initial axial load present at each of the corresponding column from gravity loads. This lead to a significant increase in the plastic moment strengths for the columns. Moreover the cracking ratios for a) beams b) external columns c) internal columns were increased "artificially" in order to ensure a similar period. The proportioning of the ratios EI_{cr}/EI_g for each of the three categories of elements was $0.60, 0.67$ and 1.00.

4.4   Conclusion

As can be seen from Figure 4.4, the lumped plasticity model yields now the same maximum base shear with the fiber model of choice. More importantly, the pre-capping equilibrium paths of the two models match well, with ultimate peak roof drifts for the fiber and lumped model are $dr_u^f = 2.548\%$ and $dr_u^l = 2.412\%$ respectively. Those drift values correspond to the maximum base shear. In addition and according to the graph, both models yield when peak roof displacement reaches a value of $\approx 5\ in$. The base shear at yield level matches also well, with the one that corresponds to the lumped model being approximately 70 $kips$ larger. This is due to the cracked stiffness ration proportioning. The stiffer the model, the higher the yield base shear, the lower the yield peak roof displacement.
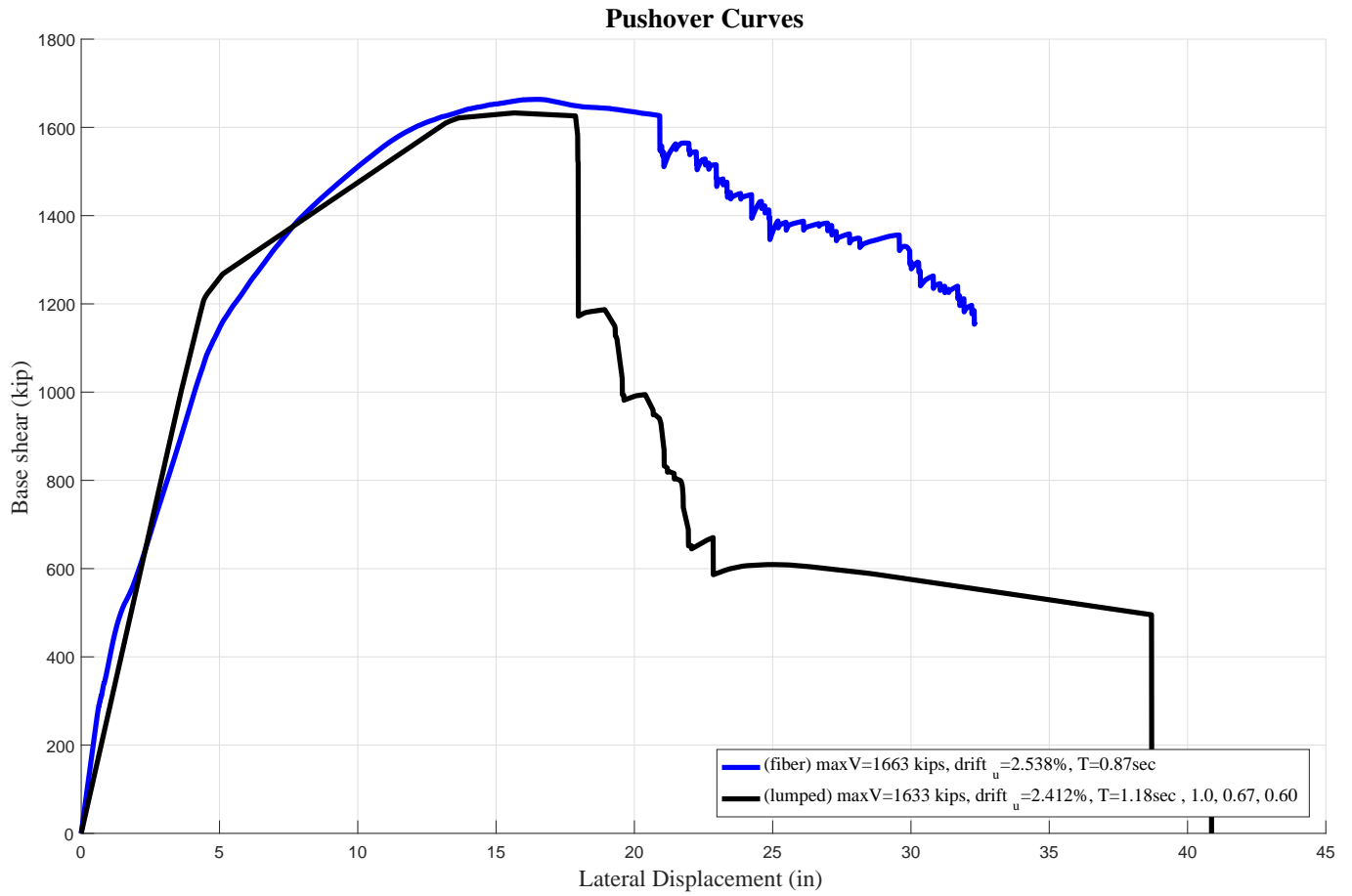
Pushover Curves

Figure 4.4: Fiber and refined lumped plasticity model response

Chapter 5

Incremental Dynamic Analysis and Assessment

5.1 Procedure Overview

In this section the results from the Incremental Dynamic Analysis will be presented, followed by an assessment of the performance for the given objectives. For the Incremental Dynamic Analysis and the assessment, the lumped model was used, since the fiber model would not converge.

5.1.1 IDA curve

An IDA curve is the result of a sequential dynamic (time-history) analysis of a given structure. For a given accelerogram, an intensity measure (IM) is chosen as independent variable (usually the acceleration). A scale factor λ is used to scale the accelerogram and obtain the next solution point. The IDA curve is the mapping between the chosen IM and a selected Engineering Demand Parameter (EDP) (e.g. max interstory drift, max chord rotation).

5.1.2 Set of IDA curves

Since IDA results in a set of solution points, which are then interpolated by a smooth curve, it is clear that structural performance cannot be assessed solely by one curve. Having multiple accelerograms can provide a more accurate representation of the response. By conducting IDA for each accelerogram, the response for a given IM is (usually) upper and lower bounder, thus, with sufficient number of curves, a safer and more credible assessment can be delivered. In this work, 44 accelerograms were used.
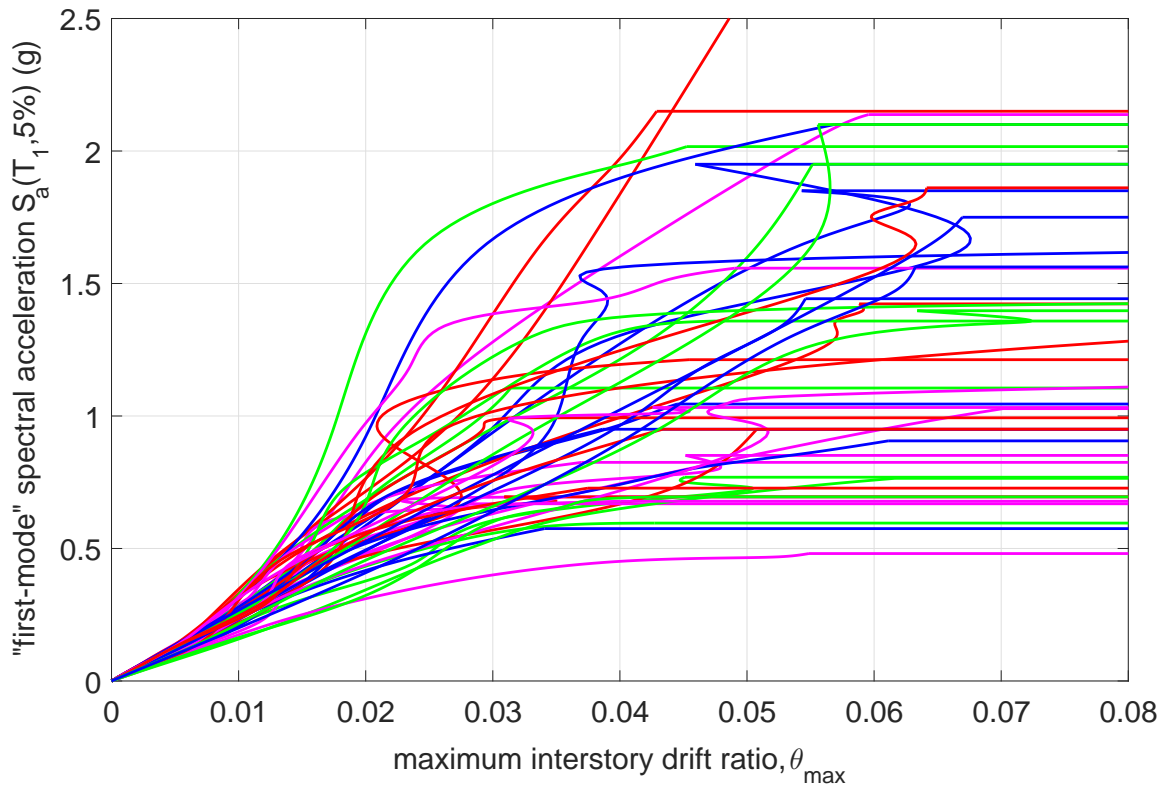

Figure 5.1: Set of 44 IDA curves for the lumped model

5.1.3 IDA fractile curves

In order to process the results, we create three distinct classes of curves: the mean, 16% and 84% fractiles. Given a certain IM, using the fractiles we can extract the percentage of the responses that remain *below* a certain EDP, which is determined by the intersection of the specific curve and the horizontal line at the level of the IM. Below the fractile curves for the following EDPs: a) the peak roof drift,b) the peak interstory drift and c) the beam maximum positive and negative hinge rotation. Beam 1 is a first story beam.
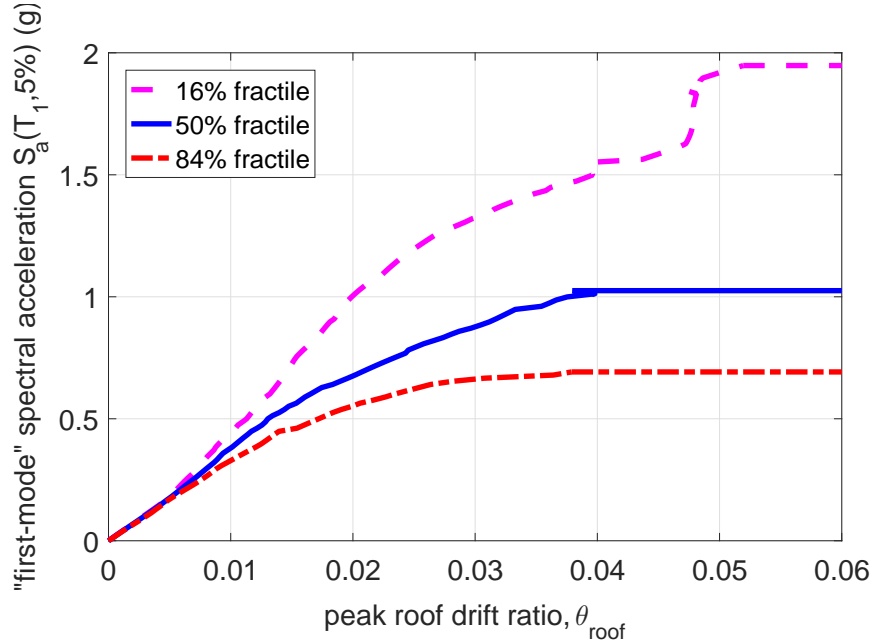

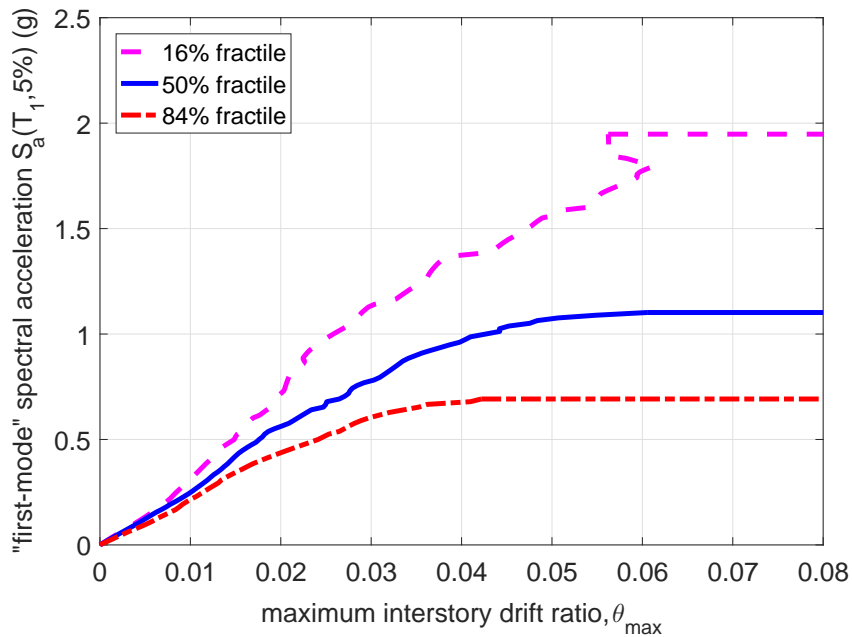Figure 5.2: IDA $16\%,50\%$ and 84% fractiles

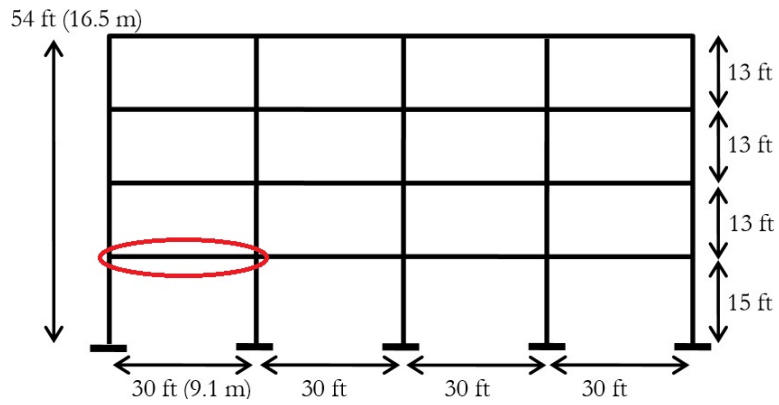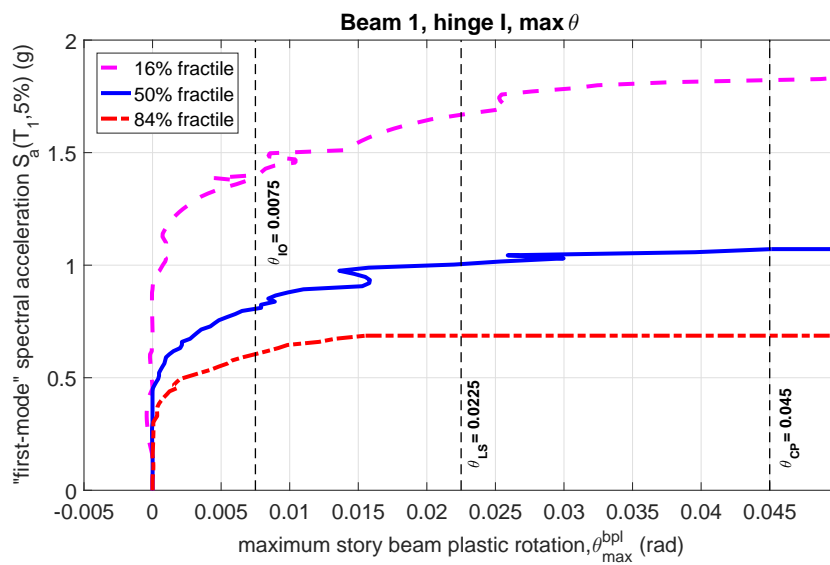Figure 5.3: IDA fractiles for max IDR

Figure 5.4: Beam 1

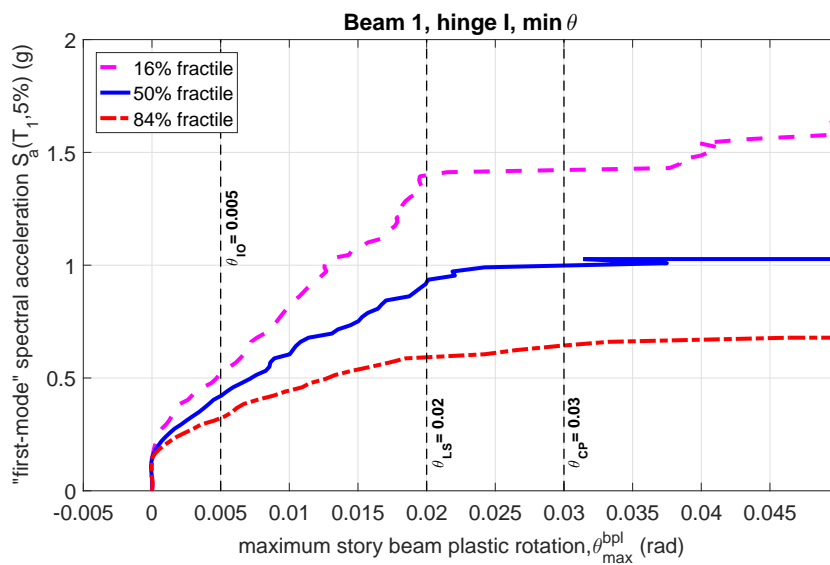Figure 5.5: IDA fractiles for max rotation of beam 1

Figure 5.6: IDA fractiles for min rotation of beam 1

5.1.4 Performance Objectives

The following performance objectives will be examined if met:

- MAF of interstory drift exceeding 2% of the story height $= 2.11 \cdot 10^{-3}$

- MAF of beam plastic hinge rotations exceeding capacities for the IO,LS and CP performance levels $2.11 \cdot 10^{-3}$

Normally, the MAFS that correspond to the LS and CP should be lower, that is, with lower frequency, however we were not provided with the corresponding values.

The performance levels for beam 1 (leftmost beam of first story) are taken from ASCE SEI-41 table X for beam hinges criteria.

Table 17.2 Modeling and acceptance criteria for **beam** plastic hinges (excerpted from ASCE SEI 41 Table 10-7 (2013)).

Condition		Modeling parameters*			Acceptance Criteria*		
$\dfrac{\rho - \rho'}{\rho_{bal}}$	$\dfrac{V}{b_w d \sqrt{f_c'}}$ †‡	Plastic rotation angle, radians		Residual strength ratio	Acceptable plastic rotation angle, radians		
		a	b	c	Performance Level		
					IO	LS	CP
≤ 0.0	≤ 3 (0.25)	0.025	0.05	0.2	0.010	0.025	0.050
≤ 0.0	≥ 6 (0.50)	0.02	0.04	0.2	0.005	0.020	0.040
≥ 0.5	≤ 3 (0.25)	0.02	0.03	0.2	0.005	0.020	0.030
≥ 0.5	≥ 6 (0.50)	0.015	0.02	0.2	0.005	0.015	0.020

f_c' in psi (MPa) units
*Values between those listed in the table should be determined by linear interpolation.
† The strength provided by the hoops (ϕV_s) must be at least three-fourths of the design shear, V.
‡ V is the design shear unless determined by a nonlinear analysis.

5.2   Assessment

Due to the limited time we had in our disposal, only the IDR and the beam 1 right end plastic hinge rotations will be assessed. For the assessment, the Hazard Curve is extracted from the Uniform Hazard Surface of San Jose, California, that corresponds to the period of the lumped model.

5.2.1   Fragility Curves

A fragility curve provides the probability of exceedance for our system, of a certain performance objective for a given IM. For maximum interstory drift levels of 1%, 2% amd 3%, the following fragility curves can be derived:
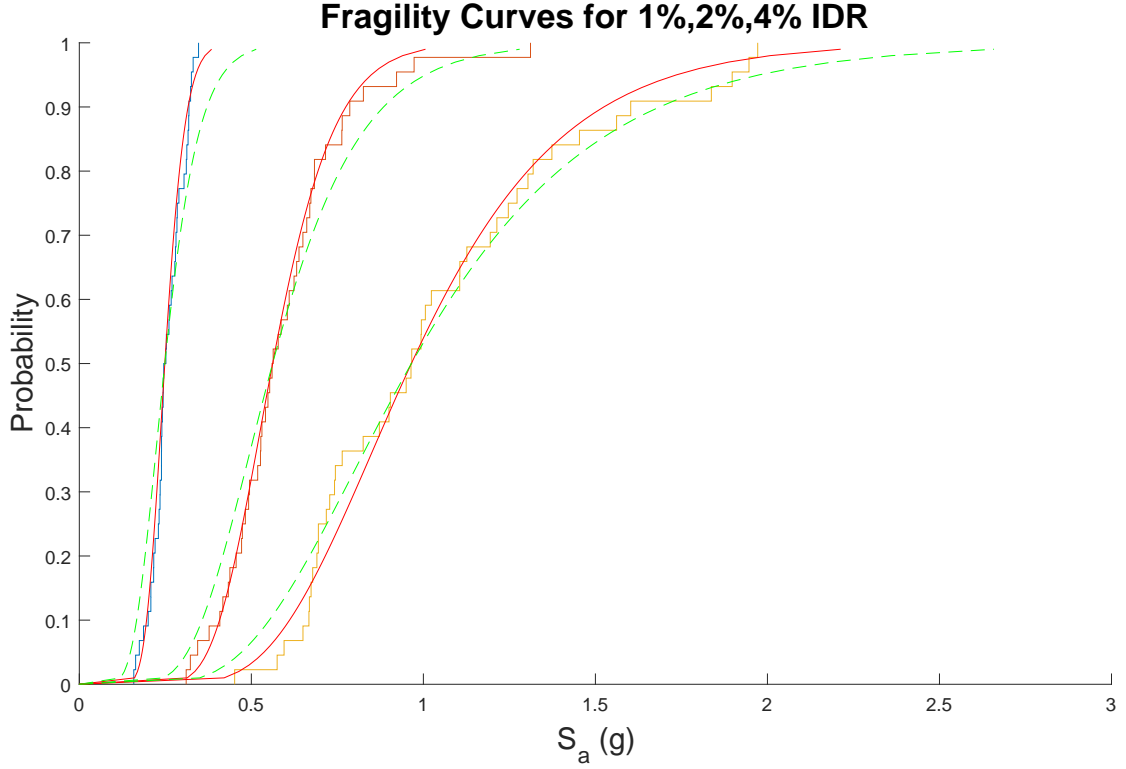
Figure 5.7: Fragility Curves for 3 different IDR levels

Each curve is the expression of the cumulative distribution function (CDF) of the standard normal distribution. For s being an intensity measure we have:

$$F_{IDR\%} = P[S_a <= s_a] = \Phi(\frac{\ln s_a - \ln S_a^{50\%}}{\beta_{S_a}})$$

where β_{S_a} is the total uncertainty and is given by the formula:

$$\beta_{S_a} = \sqrt{\beta_{S_a}^2 + \beta_{US_a}}$$

with $beta_{S_a}$ and β_{US_a} representing a) the variance of the fractile IDA curves and b) various systemic uncertainties that cannot be easily included in the formalism. A value of 25% for the later, whereas the first will be determined for the case of 2% IDR (Figure 5.8).
For this case, the variance can be calculated in the following manner:

$$\beta_{S_a} = \frac{ln S_a^{84\%} - ln S_a^{16\%}}{2} \approx \frac{ln 0.75 - ln 0.42}{2} = 0.580$$

Thus, the total uncertainty is $\beta_{S_a} = \sqrt{0.25^2 + 0.58^2} \cong 63\%$
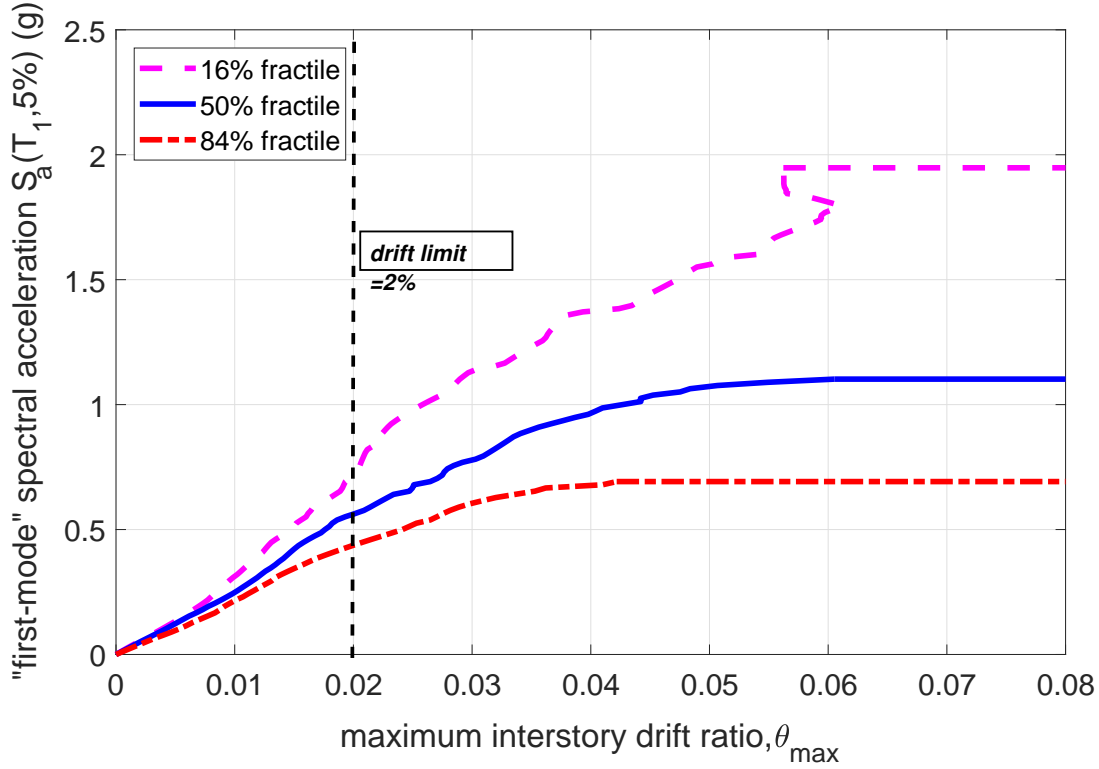
Figure 5.8: IDA curves and $EDP = 2\%$

5.2.2 Hazard Curve

The hazard curve of a certain region provides a quantitative representation of the seismic hazard. For a certain period, it maps the Intensity Measure to a mean annual frequency of exceedance of this IM. For our targets, the MAF lower than that specified in the Section **4.1.4**, which represents the mean period of the earthquake that causes equal or greater EDP: $T_e = 1/MAF_{LS} = 1/(2.11 \cdot 10^{-3}) = 475 \; years$.

The MAF of exceedance of our objectice can be calculated numerically by combining fragility and hazard curve according to the following formula:

$$MAF_{obs} = \int_0^\infty P(C < D\|s) \cdot |dH(s)| < MAF_{LS}$$

where $P(C < D\|s)$ represents the fragility given a level of EDP and $H(s)$ is the seismic hazard function.

Maximum Interstory Drift

As can be seen from the nexti figure, the objective of $MAF(IDR > 2\%) < MAF_{LS} = 2.11 \cdot 10^{-3}$ is not met.
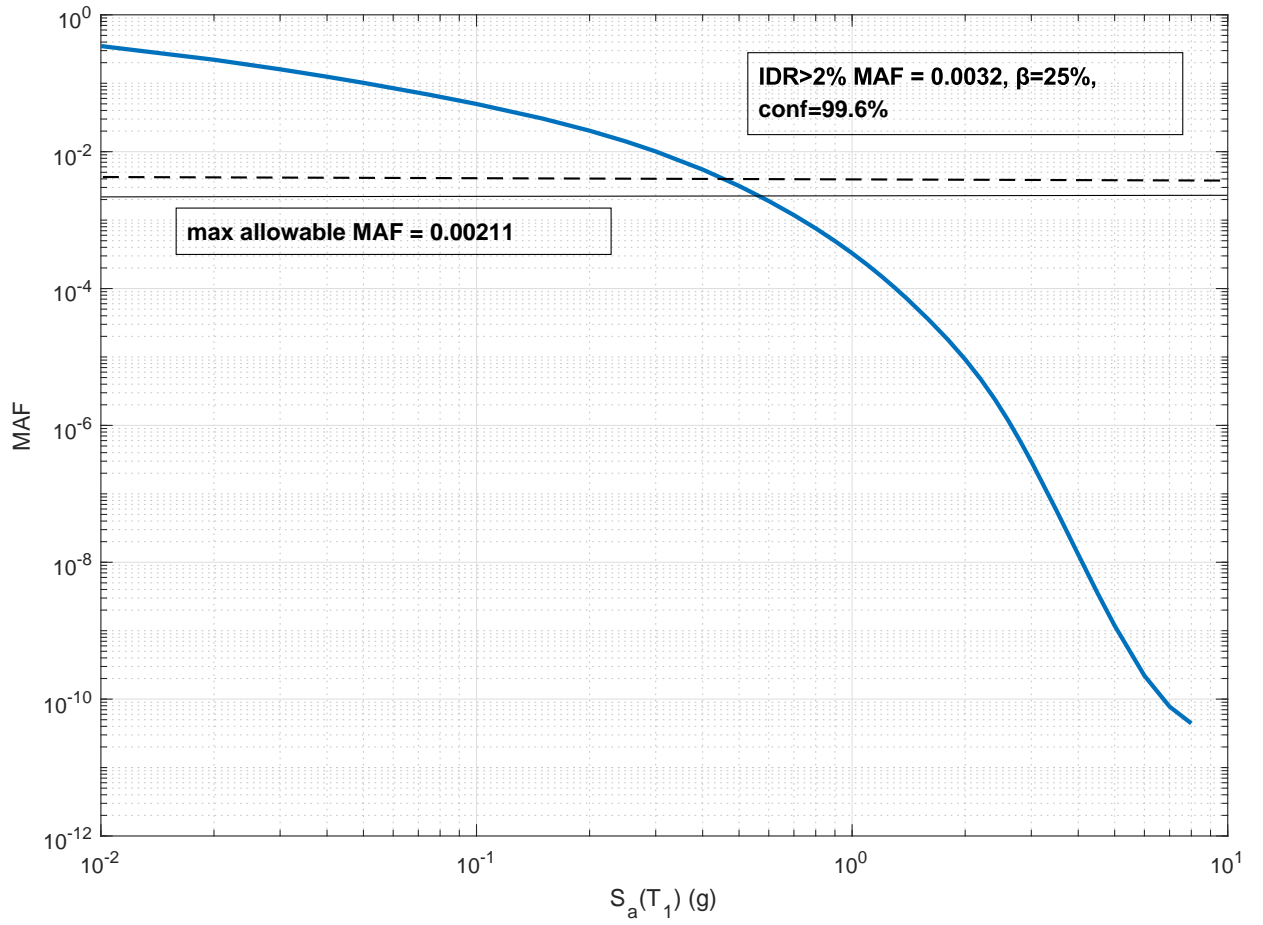
Figure 5.9: Hazard curve and IDR

Beam 1,Section I max-min rotation

For the left end of Beam 1, the following acceptance criteria are derived with linear interpolation from Table 10-7 ASCE SEI:

Table 5.1: Acceptance criteria for Beam 1, Hinge I for IO,LS and CP levels

Fractile	IO	LS	CP
$S_a^{84\%}$	0.604	0.687	0.687
$S_a^{50\%}$	0.810	1.003	1.071
$S_a^{16\%}$	1.401	1.676	1.827
$\boldsymbol{MAFS}$	**0.0018**	**0.0010**	**0.0010**

As we can see, Beam 1 rotation also fail to pass the performance objectives for all three limit states. However, it should be highlighted again that the $MAF_{LS} = 2.11 \cdot 10^{-3}$ is common to all targets, when in fact it corresponds mainly to the CP limit state.
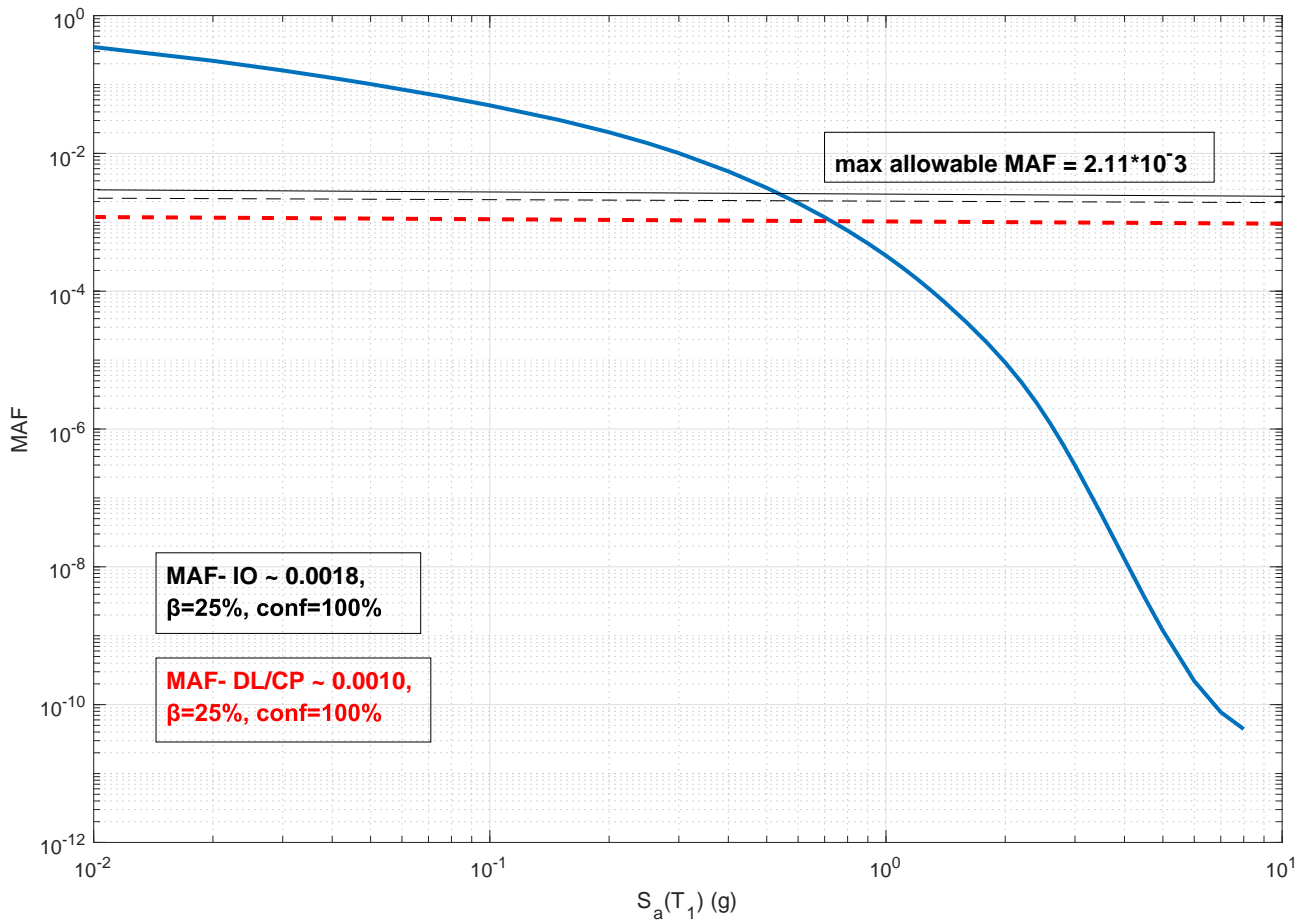
Figure 5.10: Hazard curve and positive rotations for Beam 1

5.3 Conclusion

From the preceding analysis it is concluded that, in contrast with the non-linear static analysis, none of the performance objectives were met. This concerns only the max IDR and a representative section of a first story beam. However, all first story beams are expected give the same results, as the frame is symmetric and the beams have the same dimensions and steel rebar configuration.

Bibliography

[1] Dimitrios Vamvatsikos, C.Allin Cornell ,*Incremental Dynamic Analysis,* Earthquake Engng.Struct.Dyn, 2001

[2] Dimitrios Vamvatsikos, Mark.A.Aschheim ,*Performance-based seismic design via Yield Frequency Spectra,* Vienna Congress on Recent Advances in Earthquake Engineering, Austria, 2013

[3] Dimitrios Vamvatsikos, Evangelos I.Katsanos, Mark A. Aschheim ,*A case study in performance-based design using yield frequency spectra,* SECED 2015 Conf. : Earthquake Risk and Engineering towards a Resilient World, Cambridge, UK, 2015

[4] http://opensees.berkeley.edu/wiki/index.php/Main_Page *, OpenSeesWiki*

[5] Zacharias D. Chavdoulas , *Σχεδιασμός Βάσει επιτελεστικότητας τετραώροφου μεταλλικου πλαισιακού κτιρίου με Φάσματα Συχνότητας Διαρροής,* MSc Thesis, National Technical University of Athens, Greece, Athens, 2015

[6] Luis F. Ibara , *Global Collapse of Frame Structures under seismic excitations* PhD Dissertation, Stanford University, 2003

[7] Keith Porter, Robert Kennedy, Robert Bachman , *Creating Fragility Functions for Performance-Based Earthquake Engineering,* Earthquake Spectra, Volume 23, No2, May 2007